© 2020. Published by The Company of Biologists Ltd | Journal of Cell Science (2020) 133, jcs249037. doi:10.1242/jcs.249037

RESEARCH ARTICLE

The cationic amino acid exporter Slc7a7 is induced and vital in zebrafish tissue macrophages with sustained efferocytic activity

Doris Lou Demy[1,2,¶], Mireille Carrère[1,2,¶], Ramil Noche[1,2,*,¶], Muriel Tauzin[1,2,‡], Marion Le Bris[1,2], Chooyoung Baek[1,2,§], Ignaty Leshchiner[3], Wolfram Goessling[4] and Philippe Herbomel[1,2,]**

ABSTRACT

Most tissues harbor a substantial population of resident macrophages. Here, we elucidate a functional link between the Slc7a7 cationic amino acid transporter and tissue macrophages. We identified a mutant zebrafish devoid of microglia due to a mutation in the *slc7a7* gene. We found that in Slc7a7-deficient larvae, macrophages do enter the retina and brain to become microglia, but then die during the developmental wave of neuronal apoptosis, which triggers intense efferocytic work from them. A similar macrophage demise occurs in other tissues, at stages where macrophages have to engulf many cell corpses, whether due to developmental or experimentally triggered cell death. We found that Slc7a7 is the main cationic amino acid transporter expressed in macrophages of zebrafish larvae, and that its expression is induced in tissue macrophages within 1–2 h upon efferocytosis. Our data indicate that Slc7a7 is vital not only for microglia but also for any steadily efferocytic tissue macrophages, and that *slc7a7* gene induction is one of the adaptive responses that allow them to cope with the catabolism of numerous dead cells without compromising their own viability.

KEY WORDS: Macrophages, Microglia, Efferocytosis, Zebrafish

INTRODUCTION

Most tissues in vertebrates harbor resident macrophages. They are thought to be important for tissue homeostasis (Okabe and Medzhitov, 2016). They display quite diverse phenotypic traits among different tissues, which historically led to them being given different names; for example, 'microglia' for the resident macrophages of the central nervous system (CNS). Many of these tissue-resident macrophages do not derive from monocytes produced in the bone marrow. Instead, they originate from the yolk sac, and migrate to colonize embryonic tissues, where they are ultimately maintained or self-renew throughout life (Perdiguero and Geissmann, 2016).

In the past years, several studies aimed at obtaining a more comprehensive view of the molecular requirements for the early establishment of microglia and tissue-resident macrophage populations in general, have been undertaken using the zebrafish model. Thus, the CSF-1 receptor and its ligand IL34 were found to be essential for the attraction of yolk sac-derived macrophages to the cephalic tissues, and the subsequent establishment of primitive microglia as well as epidermal macrophages (Herbomel et al., 2001; Wu et al., 2018). In addition, developmental neuronal cell death was also found to be important for microglia establishment in the midbrain optic tectum (Xu et al., 2016). In parallel, we and others performed forward genetic screens for zebrafish larvae devoid of microglia (Demy et al., 2017; Meireles et al., 2014; Rossi et al., 2015; Shiau et al., 2013) based on the convenient technique of staining of microglia in live zebrafish larvae with Neutral Red that we introduced (Herbomel et al., 2001). The mutations causing microglia absence published so far all affected microglia or their precursors cell autonomously and encoded proteins with very diverse functions – a Nod-like cytoplasmic receptor (Nlrc3l/Nlrp12), a transmembrane phosphate exporter (Xpr1b), a nuclear transcription regulator (Trim33), and a transmembrane cationic amino acid transporter (Slc7a7). For most of them, it is still unclear how the causative mutation leads to microglia absence. We originally found the *slc7a7* mutant in a screen performed together with F. Peri's team, who have then published their study, which concluded that Slc7a7 identifies microglial precursors prior to entry into the brain (Rossi et al., 2015) and microglia thereafter. While our independent mapping of the mutation agreed on the nature of the causative mutation, our conclusions on the functional significance of Slc7a7 in microglia development are quite different. Therefore, we present here our own study. In short, we show that *slc7a7* expression is induced in any efferocytic tissue macrophages in the zebrafish larva, and is vital for them whenever they have to provide a high rate of efferocytic activity. Our study also sheds light on how microglia acquire some of their long-term specific molecular signature.

RESULTS

In an F3 screen following N-ethyl-N-nitrosourea (ENU)-based mutagenesis, we identified *cerise*^{NO067} – hereafter referred to as *cerise* – as a recessive mutant that displayed no microglia vitally stained by Neutral Red (NR) at 4 days post fertilization (dpf) (Fig. 1A,B). *Cerise* mutants are still devoid of microglia by 9 dpf (Fig. 1C) but otherwise properly developed, with a swim bladder and robust blood circulation (Fig. S1A,B), and can survive for up to 17 days (data not shown).

We first mapped the *cerise* mutation by bulk segregant analysis of simple sequence length polymorphisms (SSLPs) (Geisler et al., 2007) to a 7.7 Mb interval on linkage group 7 (LG7). We then moved to single nucleotide polymorphism (SNP) analysis based on whole-genome sequencing (Leshchiner et al., 2012) of pools of mutant and sibling embryos (three pools; 20 siblings, 20 mutants, then 200 mutants). This analysis refined the location of the causative mutation within the previously defined region of LG7, and led to the

[1]Institut Pasteur, Department of Developmental & Stem Cell Biology, 75015 Paris, France. [2]CNRS, UMR3738, 75015 Paris, France. [3]Broad Institute of Harvard and MIT, Cambridge, MA 02124, USA. [4]Division of Gastroenterology, Massachusetts General Hospital, Harvard Medical School, Boston, MA 02115, USA.
*Present address: Zebrafish Genetics and Disease Models Facility, The Hospital for Sick Children, Toronto, M5G 0A4, Canada. ‡Present address: Direction de la Recherche Medicale et de l'Innovation, CHU de Toulouse, 31059 Toulouse cedex 9, France. §Present address: Ecole de l'Inserm Liliane Bettencourt, 75013 Paris, France.
¶These authors contributed equally to this work

**Author for correspondence (philippe.herbomel@pasteur.fr)

M.L., 0000-0002-6649-7836; P.H., 0000-0002-8946-3313

Handling Editor: Daniel Billadeau
Received 21 May 2020; Accepted 9 September 2020

Journal of Cell Science (2020) 133, jcs249037. doi:10.1242/jcs.249037

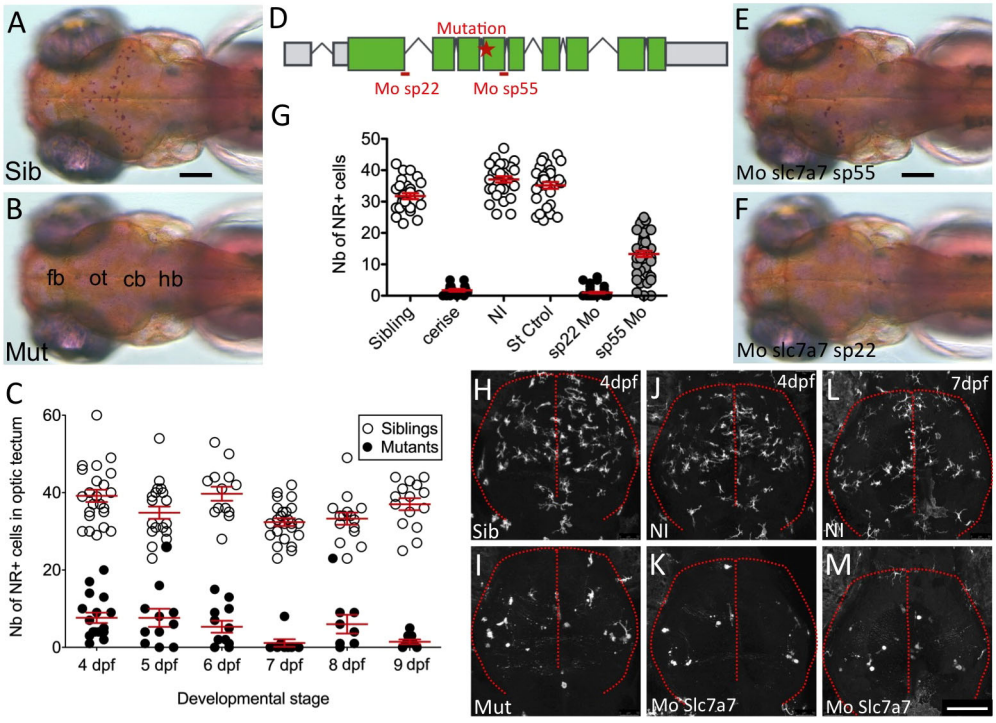

Fig. 1. The *cerise* phenotype of microglia absence is caused by a mutation in the *slc7a7* gene and is fully mimicked by the sp22 morpholino. (A,B) Dorsal view of the microglia in the optic tectum of live 4 dpf larvae stained with NR in siblings (A) and *cerise* mutants (B). (C) Quantification of NR+ tectal microglia in *cerise* sibling (white dots, *n*=112) and mutant (black dots, *n*=66) larvae from 4 to 9 dpf. (D) Exon structure (green boxes) of the *slc7a7* gene, with position of the *cerise* mutation (red star) and of the splice junctions targeted by the sp22 and sp55 morpholinos (red dashes). (E,F) Dorsal view of the tectal microglia in live NR-stained sp55 (E) and sp22 (F) morphant larvae at 4 dpf. (G) NR+ tectal microglia cell counts (at 4 dpf) show that, unlike what is seen for sp55, the sp22 morpholino fully mimics the absence of microglia of *cerise* mutant larvae. This experiment was done 7 years after the one shown in C; the overall stronger mutant phenotype here is likely due to the selection of carriers leading to clear mutant phenotypes over fish generations. (H–M) Dorsal view (rostral to the top) of mCherry+ tectal microglia in *Tg(mfap4:mCherryF)* zebrafish larvae at 4 dpf in control siblings (H), *cerise* mutants (I), uninjected controls (J), sp22 morphants (K), and at 7 dpf in uninjected controls (L) and sp22 morphants (M). Red dotted lines indicate the brain contours and midline. Error bars in C and G show mean±s.e.m. Scale bars: 100 µm. Sib, sibling; mut, mutant; fb, forebrain; ot, optic tectum; cb, cerebellum; hb, hindbrain; NI, non-injected; Mo, morpholino; NR+, NR positive; Nb, number.

identification of a homozygous A>T transversion in the mutants at the splice junction between intron 4 and exon 5 of the gene *solute carrier family 7, member 7* (*slc7a7*) gene (Fig. 1D), confirming the results obtained by Rossi et al. (2015) in their independent characterization of the *cerise* mutant. This gene encodes the catalytic subunit of the heterodimeric transmembrane cationic amino acid (CAA) transporter y+LAT-1 (Torrents et al., 1999). The *cerise* mutation changes the final AG of intron 4 into TG, which leads to exon 5 skipping and splicing of exon 4 to exon 6, as verified by mutant cDNA sequencing (data not shown). This causes a frameshift from the beginning of exon 6, leading to a premature stop codon nine codons downstream. Hence, the predicted mutant protein comprises only the N-terminal half of the 501 amino acid wild-type (WT) Slc7a7 protein followed by 9 new amino acids, and thus lacks six of its 12 transmembrane domains.

We evaluated the expression of *slc7a7* and of the other genes encoding transmembrane CAA transport systems expressed at the plasma membrane in macrophages/microglia (Fotiadis et al., 2013), through an RNA-seq analysis that we performed on fluorescent macrophages/microglia sorted from zebrafish larvae expressing mCherry under the control of a macrophage-specific promoter (*mpeg1*) at 3 dpf (Fig. S2; Table S1). We found *slc7a7* to be expressed at a high level in these cells, for example, twice as much as the transmembrane receptor and macrophage lineage marker gene *csf1r*. In contrast, *slc7a6*, encoding the closely related y+LAT-2 transporter, was expressed very weakly. Of the three genes encoding monomeric CAA transporters – CAT-1 (*slc7a1*), CAT-2 (*slc7a2*) and CAT-3 (*slc7a3*) – only *slc7a2* and *slc7a3* were found to be expressed, but at a level 10-fold lower than that of *slc7a7* (Fig. S2 and Table S1). Thus, y+LAT1/Slc7a7 is the main CAA transporter in macrophages/microglia of zebrafish larvae.

To confirm that the *cerise* phenotype was caused by Slc7a7 deficiency and have an alternative tool to knock this gene down, we designed two different splice blocking morpholinos (Mos) (Fig. 1D). Upon injection into WT embryos, the effect of the sp55 Mo – closest to the mutation, and used by Rossi et al. (2015) – on microglia was only partial, whereas the sp22 Mo fully phenocopied the *cerise* mutation (Fig. 1E–G). Accordingly, subsequent experiments were conducted using the sp22 Mo.

Transferring the *cerise* mutation into the transgenic *Tg(mfap4:mCherryF)* background, which specifically highlights macrophages/microglia, confirmed the lack of primitive microglia from 4 dpf onwards (Fig. 1H,I; Fig. S1C,D). The same was found in *slc7a7*-sp22 morphants (Fig. 1J–M). At earlier stages (2 dpf), Slc7a7-deficient embryos display a normal production and overall deployment of primitive macrophages, and are phenotypically unrecognizable from their controls (Fig. S1E,F).

Slc7a7-deficient macrophages die after colonizing the brain and retina

We noticed that the few microglial cells occasionally seen in the optic tectum (OT) of the mutants at 4 dpf, and even more so at 3 dpf

Journal of Cell Science (2020) 133, jcs249037. doi:10.1242/jcs.249037

(when the tectal microglia is just being established in the WT – see below), were more heterogeneous in size than WT microglia, and quite often occurred in small groups at the ventro-lateral corners of the OT (Fig. S3A–D, arrows) (this trait, not seen in other microglia mutants of our collection, is actually why we initially named this mutant *cerise*). Closer examination by video-enhanced differential interference contrast (VE-DIC) microscopy revealed unusual unstained large vacuoles adjacent to or including the NR-stained material (Fig. S3E–G), that were not seen in wt larvae. Similar vacuoles appeared to be fluorescent in *cerise Tg(mfap4:mCherryF)* larvae, suggesting that they are remnants of dead/dying mCherry-positive macrophages/microglia (Fig. S3H–H″). As macrophage death in the CNS or elsewhere cannot be assessed by the usual markers of apoptosis (e.g. annexin V staining, caspase 3 activation or Tunel) because most of these cells contain engulfed dead cells that stain positive for all these markers, we turned to *in vivo* time-lapse confocal imaging. We followed the behavior of fluorescent tectal macrophage/microglial cells in transgenic morphant larvae from 3 dpf onwards and compared it to that in control larvae (Fig. 2A–C; Movies 1 and 2). While the latter displayed the typical ramified and dynamic morphology with little movement of the cell center acquired by that developmental stage (Li et al., 2012; Peri and Nüsslein-Volhard, 2008; Svahn et al., 2013), their counterpart in the morphant still displayed more-macrophage-like morphodynamics (Movies 1 and 2). Then, over the next 10 h, they disappeared from the tectum (Fig. 2A–C) – mostly after rounding up, becoming inert, and being engulfed by another macrophage/microglial cell, which a moment later also underwent the same fatal fate (Fig. 2C; Movie 2). These observations indicate that Slc7a7-deficient macrophages are actually able to colonize the OT but died once there, which could explain their inability to ever establish as a proper microglial population.

To further explore this prospect of a transient colonization of the CNS in Slc7a7-deficient embryos, we aimed to examine earlier developmental stages. The OT and the retina are the two CNS structures most densely populated with microglia in zebrafish larvae, but they acquire most of them at different times. While the main wave of OT colonization occurs between 2.5 and 3.5 dpf

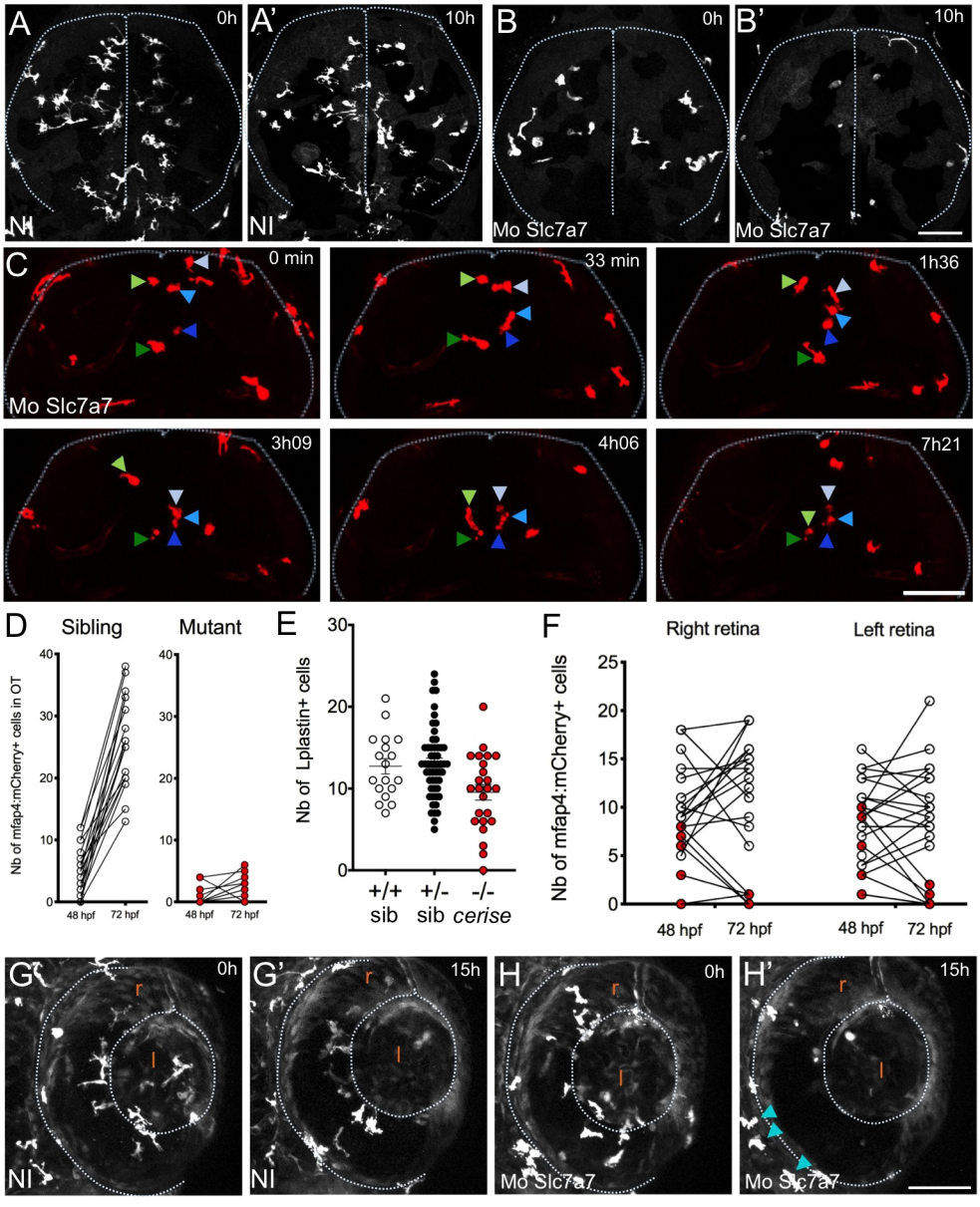

Fig. 2. Macrophages/microglia in Slc7a7 deficient larvae die within the brain and retina from 2.5 dpf onwards. (A–B′) Dorsal view (rostral to the top) of the tectal microglia in live *Tg(mpeg1:Gal4; UAS:Kaede)* zebrafish larvae at the beginning (A,B) and end (A′,B′) of a 10 h time-lapse confocal imaging session started at 72 hpf of a non-injected control (A,A′) and a sp22 morphant (B,B′). White dotted lines indicate the brain contours and midline. (C) Selected time points (maximum projections) of the *in vivo* time-lapse confocal imaging of Tg*(mpeg1: Gal4; UAS:NfsB-mCherry)* tectal microglia started at 72 hpf of a sp22 morphant; dorsal view, rostral to the top. Grey or blue arrowheads, and green arrowheads, point at two series of macrophages that die, are engulfed by another, which then dies in turn, and so on; see also Movie 2. White dotted lines indicate the brain contours. (D) *In vivo* quantification of mCherry+ macrophages/microglia in the OT of *Tg(mfap4:mCherryF) cerise* siblings (white dots) and mutants (red dots) examined sequentially at 48 and 72 hpf. (E) Quantification of L-plastin+ macrophages in the retinas of *cerise* progeny at 42 hpf, immunostained for L-plastin and subsequently genotyped as homozygous WT (+/+), heterozygous (+/−) or homozygous *cerise* mutants (−/−). Error bars show mean±s.e.m. (F) *In vivo* quantification of mCherry+ macrophages/microglia in the retina of *Tg(mfap4:mCherryF) cerise* siblings (white dots) and mutants (red dots) examined sequentially at 48 and 72 hpf. (G–H′) Lateral view of the retinal microglia of live *Tg(mpeg1:Gal4; UAS:NfsB-mCherry)* larvae at the beginning (G,H) and end (G′,H′) of a 15 h time-lapse imaging session started at 54 hpf of a non-injected control (G,G′) and a sp22 morphant (H,H′). See also Movies 3 and 4. Scale bars: 75 µm. r, retina; l, lens; NI, non-injected; Mo, morpholino; Nb, number.

Journal of Cell Science

Journal of Cell Science (2020) 133, jcs249037. doi:10.1242/jcs.249037

(Herbomel et al., 2001; Xu et al., 2016; see also Fig. 3D), the retinal microglia number has already reached its plateau by 48 hpf (Demy et al., 2017; Herbomel et al., 2001). We therefore counted the number of macrophage/microglia cells in the retinae by 42 hpf in the progeny of *cerise* heterozygote carrier fish, and then genotyped the embryos. The results demonstrated that macrophages in homozygous mutant embryos were indeed able to colonize the retinas quite efficiently (Fig. 2E). An independent live follow-up of individual embryos documented the subsequent decrease of the retinal macrophage/microglia population in the mutants between 2 and 3 dpf (Fig. 2F). Following our previous observations in the OT, we hypothesized that these retinal macrophages also died. Hence, we performed time-lapse imaging for the retinal macrophages in morphant and control embryos from 54 hpf onwards. In the time-lapse sequences shown in Fig. 2G–H″ and Movies 3 and 4, while the retinal macrophage number in the morphant was similar to the control at the onset of the imaging, it then steadily decreased, to virtually zero by 15 h later, with evidence of macrophage rounding and demise (Fig. S4A–A″). Interestingly, macrophages in interstitial tissues around the eye showed no sign of cell death (Fig. 2H′, cyan arrowheads).

Thus, it appears that Slc7a7-deficient macrophages are able to colonize the OT and retina normally, but die there, starting from 2.5 dpf. In the retina, where the microglial population has already reached its plateau by this stage, it results in a drop in cell number (Fig. 2E,F); in the OT, as the colonization wave and disappearance are concomitant, the microglial population never becomes substantial (Fig. 2D).

Neutrophils infiltrate the brain and retina of Slc7a7-deficient larvae following microglia demise

In the zebrafish embryo, beside macrophages, primitive myelopoiesis in the yolk sac also produces neutrophils. Unlike in mammals, these neutrophils then disperse, live and wander in tissues, like the macrophages, except for the CNS that they normally never enter (Le Guyader et al., 2008). However, in *cerise*/*slc7a7* mutants and morphants, we found a massive infiltration of neutrophils in the brain OT and the retinas by 4 dpf (Fig. 3A–C). Through time-lapse confocal imaging of GFP+ neutrophils in *Tg(mpx:GFP)* larvae, we found that this influx of neutrophils into the retinae and brain started by 2.5–3 dpf, when the macrophages/microglial cells were dying there (Fig. 3D–F; Movie 5). Time-lapse imaging of double transgenic lines highlighting macrophages in red and neutrophils in green confirmed the link between macrophage state and neutrophil recruitment, as the latter repeatedly interacted with the dying macrophages remaining in the *cerise* brain (Fig. 3G,H; Fig. S5). Past 4 dpf – by 6 and 9 dpf – neutrophils were less frequently observed in the CNS; whenever present, they always correlated with the presence of dying macrophages/microglia, with which they interacted (Fig. S5F–I″).

Neither quantitative (q)PCR for the cytokines that might be released by the stressed/dying macrophages (IL1-β, TNF-α and CXCL8), nor immunohistochemistry for IL1-β (Vojtech et al., 2012), nor *slc7a7* Mo injection into *Tg(IL1-β:GFP)* reporter embryos (Nguyen-Chi et al., 2014) allowed us to identify the molecular signals responsible for the attraction of neutrophils to the dying microglia in the CNS of mutant larvae, leaving them yet to be identified (data not shown).

Slc7a7 is required for the survival of highly efferocytic tissue macrophages

The above results show that microglial cells in *cerise* larvae begin to die by 2.5 dpf. This is also precisely the stage at which WT microglial cells become intensely vitally stained by NR (Herbomel et al., 2001). As a weak base, NR accumulates in the phagolysosomal compartment. In primitive microglia, it accumulates over time in the phagosomes containing apoptotic bodies that have become acidified (Fig. S6). The onset of intense NR staining of microglia by 56–60 hours post fertilization (hpf) (Herbomel et al., 2001) thus actually reflects the beginning of the major wave of neuronal developmental cell death (DCD) and the engulfment of the numerous resulting corpses by the young microglia. As microglial cells in *cerise*

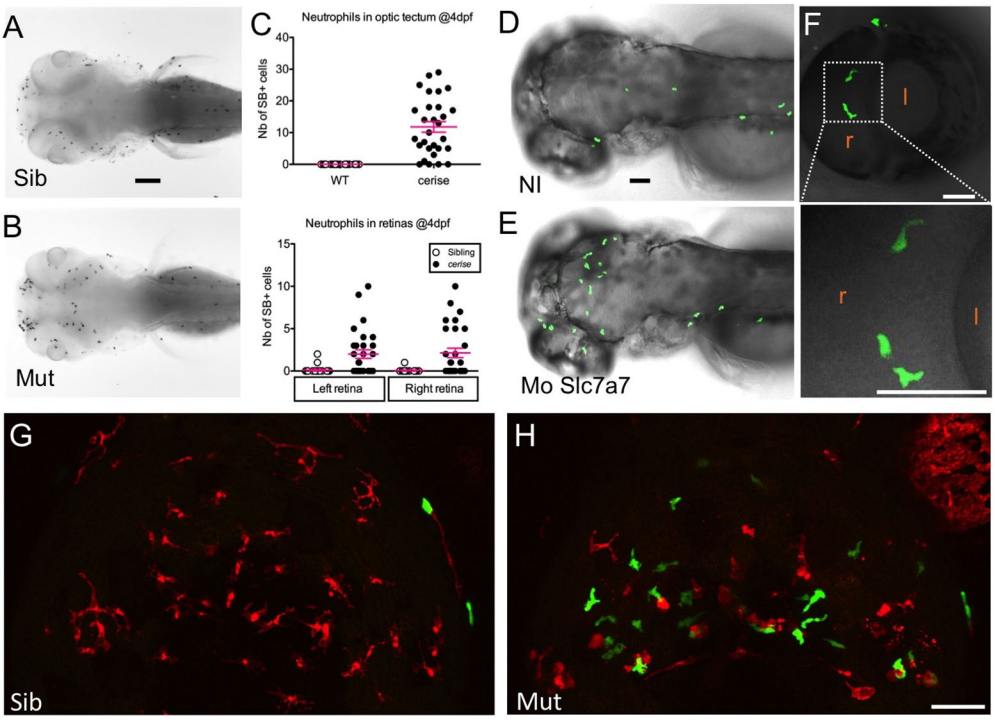

Fig. 3. Neutrophils are recruited to the CNS of Slc7a7-deficient larvae following macrophage/microglia death. (A–C) Dorsal view of control (A) and *cerise* (B) larvae at 4 dpf stained for neutrophils with Sudan Black (SB), and corresponding SB+ cell counts in the OT and retinas (C). Error bars show mean± s.e.m. (D–F) Dorso-lateral view of live *Tg(mpx:GFP)* control (D) and *slc7a7* sp22 morphant (E) larvae at 3 dpf, and close-ups on GFP+ cells within the morphant retina at 3 dpf (F). See also Movies 5 and 6. (G,H) Dorsal view, rostral to the top, of the OT of sibling (G) and mutant (H) *Tg(mpeg1:mCherry; mpx:GFP)* larvae at 4 dpf, with macrophages/microglia in red, and neutrophils in green (maximum projection of a confocal *z*-stack spanning the entire OT); see also Movies 7 and 8. Scale bars: 100 µm (A,B), 50 µm (all other panels).

Journal of Cell Science (2020) 133, jcs249037. doi:10.1242/jcs.249037

embryos begin to die by that same stage, we hypothesized that Slc7a7 could be vital for macrophages/microglia that have to eliminate numerous apoptotic cells. Indeed, our imaging did indicate that, before dying, Slc7a7-deficient microglia were capable of efferocytosis just like WT (Fig. S4B,C), and we occasionally witnessed them dying just after engulfing a neuronal or microglial cell corpse (Fig. 2C; Fig. S4D–F″). We therefore examined other tissue macrophage populations that face such a situation at some point in zebrafish development. Beside microglia, we previously noted the similarly intense but more transient NR staining of the macrophages that eliminate the remnants of the hatching gland by 3 dpf (Fig. 4A) (Herbomel et al., 2001), and the macrophages of the caudal hematopoietic tissue (CHT; Murayama et al., 2006), which engulf many of the circulating primitive erythrocytes particularly from 6 to 12 dpf (Fig. 4B,C), as the latter become progressively replaced by erythrocytes produced from the definitive hematopoiesis. Therefore, we examined these highly efferocytic macrophage populations in *cerise* mutants and their siblings. In the latter, at the hatching gland location at 3 dpf, WT mCherryF+ macrophages, despite a heavy efferocytic load, still showed numerous long pseudopodia/ramifications (Fig. 4D). In sharp contrast, in *cerise* mutants, no ramified macrophages could be seen, and the widely scattered mCherryF+ spots, mostly of subcellular size, were strongly suggestive of macrophage degeneration (Fig. 4E). Similarly, in the CHT, *cerise* mutants display an accumulation of subcellular-sized mCherry+ spots and many fewer healthy macrophages than in WT controls (Fig. 4F–I).

These data collected across tissues and stages, taken together, strongly suggest that *slc7a7* expression is vital for any tissue-resident macrophages that even transiently face the challenge of intense efferocytic work.

We further explored this hypothesis by inducing large-scale efferocytic work for macrophages in *slc7a7* Mo and control embryos. To achieve this, we took advantage of the fact that blood circulation in zebrafish embryos is open until 2.5 dpf (due to its free flow in the yolk sac before the closure of the common cardinal vein) and thus readily accessible to all interstitial macrophages. We treated embryos at 30 hpf for 20 h with a low dose of phenylhydrazine (PHZ), which induces apoptosis of all circulating primitive erythrocytes (Ferri-Lagneau et al., 2012; Shafizadeh et al., 2004). Macrophages in *slc7a7*-sp22 morphants readily engulfed the apoptotic erythrocytes within a few hours as in WT control embryos, but on the next day, they had virtually disappeared from the *slc7a7* morphant embryos treated with PHZ, while their number had only slightly decreased in the control embryos (Fig. 4J–L).

Slc7a7 expression is induced in tissue macrophages upon efferocytosis

We next examined the expression of the *slc7a7* gene in wt larvae by whole-mount *in situ* hybridization (WISH) (Fig. 5). We noticed that the two tissue macrophage populations that showed a distinctly higher *slc7a7* expression by WISH were precisely the brain and retinal macrophages/microglia from 56 hpf onwards

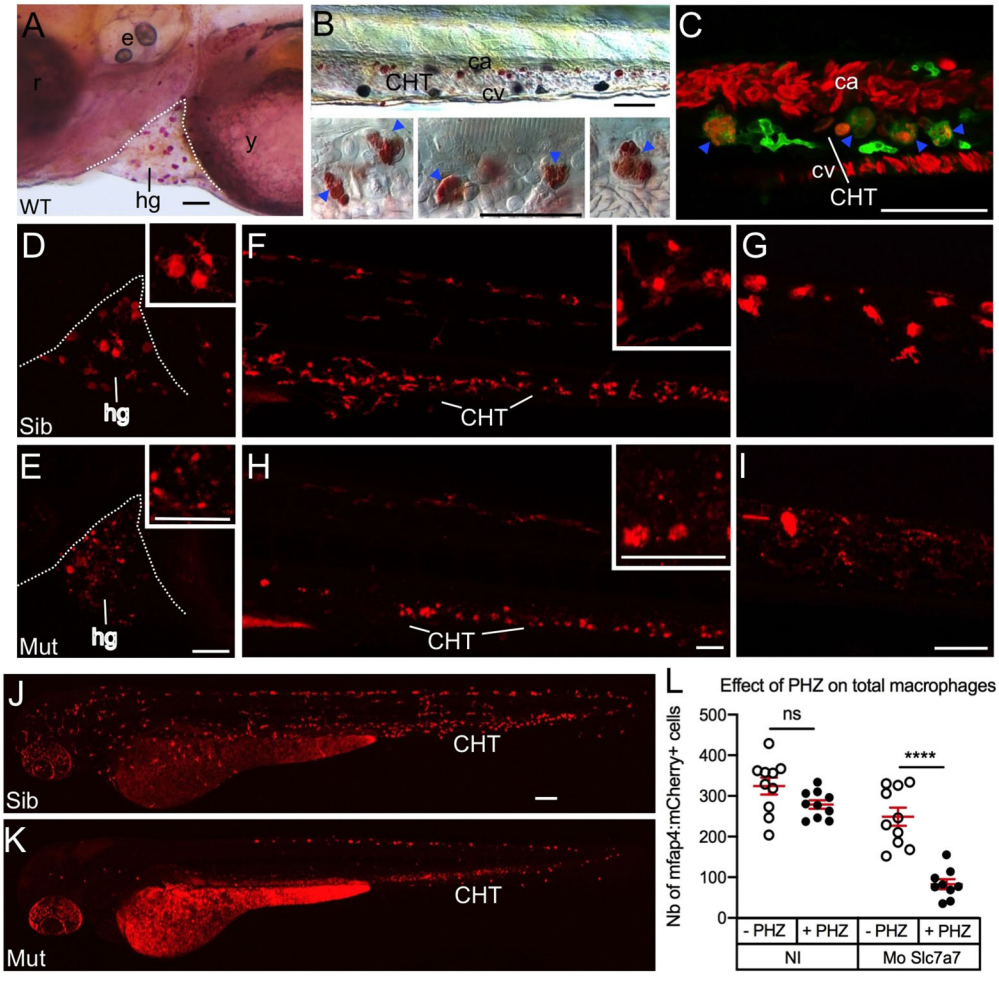

Fig. 4. Tissue macrophages other than microglia also die upon sustained efferocytosis in *cerise* mutants. (A–C) Lateral view of the hatching gland (hg) at 3 dpf (A) and CHT at 7 dpf (B,C) in live WT larvae vitally stained with NR (A,B), or in a *Tg(gata1: DsRed; mpeg1: GFP)* larva (C). (D–I) Comparative lateral views of the red fluorescence of sibling (Sib, D,F,G) and mutant (Mut, E,H,I) *Tg(mfap4:mCherry)* or *Tg(mpeg1:mCherry)* larvae, showing the hatching gland (hg) at 3 dpf (D,E), the CHT at 3 dpf (F,H), and the CHT at 6 dpf (G,I). White dotted lines indicate the limits of the hatching gland. (J–L) Lateral view of the global macrophage population at 54 hpf in live *Tg(mpeg1: mCherryF)* control (J) and *slc7a7* morphant (K) embryos treated with PHZ at 30 hpf for 20 h, and corresponding quantification (L). Error bars show mean±s.e.m. ****P<0.0001; ns, not significant (P>0.05) (two-way ANOVA). Scale bars: 50 µm. y, yolk sac; ca, caudal artery; cv, caudal vein.

Journal of Cell Science (2020) 133, jcs249037. doi:10.1242/jcs.249037

(i.e. the stage at which neuronal DCD begins) and the hatching gland-associated macrophages by 3 dpf (Fig. 5A–C). From 3 dpf, again consistent with the death of Slc7a7-deficient macrophages, the *slc7a7* mRNA signal was also lightly detected in the tail (Fig. 5D), in addition to the kidney tubules and gut epithelium, as in mammals (Fig. 5E).

We then examined *slc7a7* expression by WISH following PHZ-mediated death and engulfment of circulating erythrocytes, and found that it was again induced in the engulfing macrophages throughout the venous system (Fig. 5F–K), enough to cause an ∼3-fold increase at the whole-embryo level (Fig. 5L). Taken together, these results indicate that *slc7a7* expression is not only required in macrophages with sustained efferocytic activity, but is also induced by the latter, suggesting that a high level of Slc7a7 is necessary in this situation.

In order to refine the temporal link between efferocytosis and upregulation of Slc7a7 expression in macrophages, we aimed to induce efferocytosis at precise anatomical locations and time. To do so, we exposed the fish embryos to a low concentration of $CuSO_4$ (50 µM), which has been shown to rapidly and specifically induce apoptosis of the sensory cells of the neuromasts of the lateral line within the epidermis (Fig. 6A), causing the immediate recruitment of five to six macrophages per neuromast to engulf the dead cells (Carrillo et al., 2016; Olivari et al., 2008). We treated the fish embryos at 54 hpf for 30 min. and monitored *slc7a7* expression at each neuromast of the posterior lateral line by WISH every 30 min over the next 6 h (Fig. 6B). The $CuSO_4$ treatment efficiently destroyed the sensory cells (Fig. 6C–E), hence recruiting macrophages (Fig. 6C′–E′), which started to express *slc7a7* strongly enough to be detected by WISH (Fig. 6C″–G), with a peak by 1.5 h post treatment (hpt), and virtually no more expression by 4 hpt (Fig. 6B), even though recruited macrophages were still present in the area (see also Carrillo et al., 2016).

Taken together, our results thus show that the cationic amino acid exporter Slc7a7 is vital for and induced in tissue macrophages with sustained efferocytic activity.

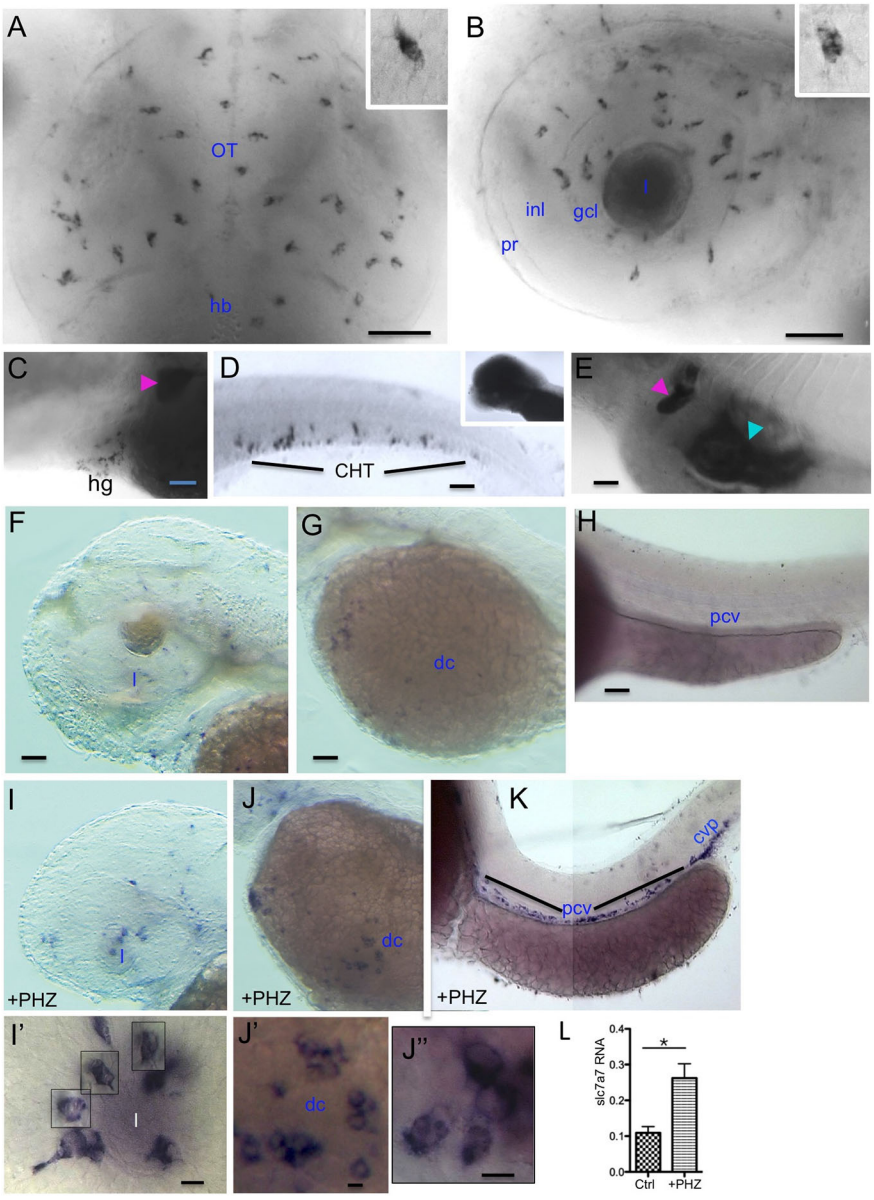

Fig. 5. Efferocytic macrophage populations strongly express Slc7a7. Whole-mount *in situ* hybridization for *slc7a7* mRNA in WT embryos. (A) Dorsal and (B–K) lateral views. (A) Optic tectum (OT), rostral to the top, 3 dpf. hb, hindbrain. (B) Retina, 60 hpf, with its concentric neuronal cell layers – ganglion cell layer (gcl), inner nuclear layer (inl) – and photoreceptor layer (pr). l, lens. Inset, close-up of a *slc7a7*+ microglial cell, showing the signal-free efferophagosomes within the cell. (C) Hatching gland (hg), 3 dpf. (D) CHT, 3 dpf; this lower *slc7a7* mRNA signal was seen when the anterior part was overexposed (inset). (E) Pronephric tubules (pink arrowhead, also visible in C) and intestinal bulb and tract (cyan arrowhead), 3 dpf. (F–L) Induction of *slc7a7* expression in macrophages following PHZ treatment. Lateral views at 50 hpf in control (F–H) or PHZ-treated (I–K) embryos. (F,I,I′) Head, with *slc7a7*+ macrophages in hyaloid vasculature behind the lens (l) in I,I′. (G,J–J″) Yolk sac, with *slc7a7*+ macrophages in the blood circulation valley (duct of Cuvier, dc) in J–J″. The higher magnification views in I′,J′,J″ show the *slc7a7*-negative efferophagosomes within the *slc7a7*+ macrophages; in I′, images of three macrophages taken at slightly different foci were superimposed on the main image so as to show them in focus. (H,K) Trunk-tail, with *slc7a7*+ macrophages in the posterior cardinal vein (pcv) and caudal vein plexus (cvp) in K. (L) Global quantification of *slc7a7* RNA expression by qPCR on control and PHZ-treated embryos. Error bars show s.e.m. **P*<0.05 (one-way ANOVA). Scale bars: 50 µm, except (I′,J′J″), 10 µm.

Journal of Cell Science (2020) 133, jcs249037. doi:10.1242/jcs.249037

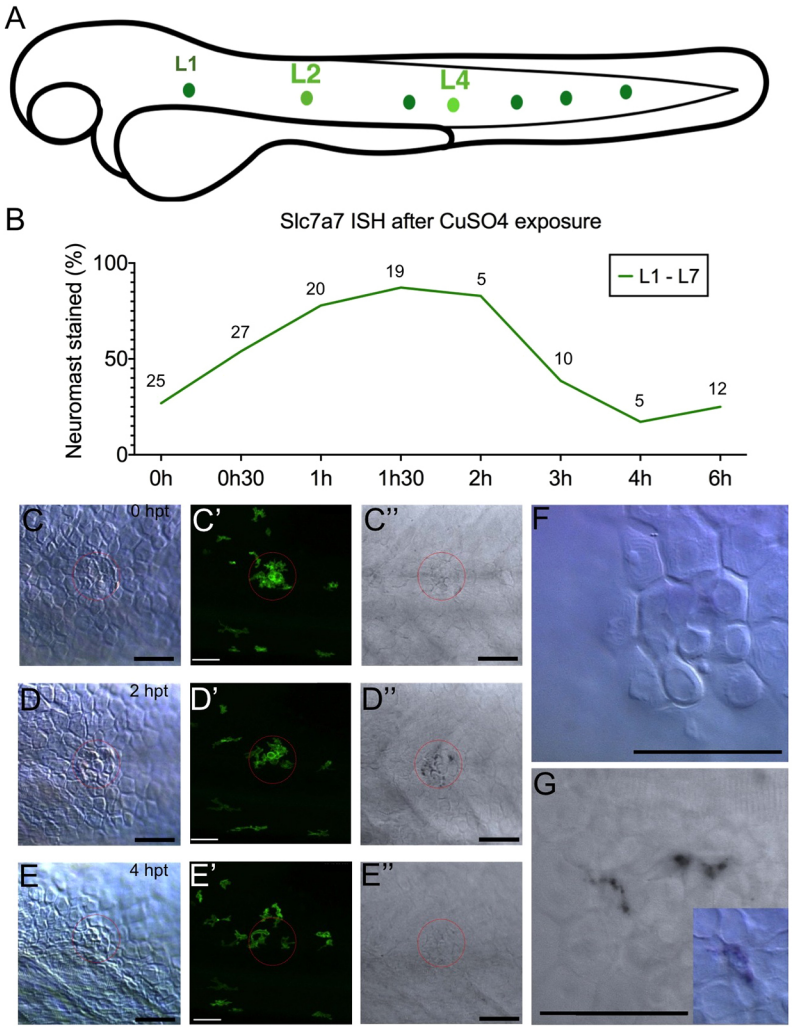

Fig. 6. Slc7a7 expression is maximally induced 1-2 h following efferocytosis. (A) Location of the neuromasts of the posterior lateral line – named L1 to L7 in the rostro-caudal direction – in the zebrafish embryo at 48 hpf. (B) Fraction of neuromasts showing a clear *slc7a7* mRNA signal by whole-mount *in situ* hybridization at successive time points after a 30 min exposure to $CuSO_4$. The number of embryos screened for each time point (*n*) is indicated above the curve. (C–G) VE-DIC/Nomarski (C,D,E,F), confocal (C′,D′,E′) and bright-field observation (C″,D″,E″,G) of neuromast morphology (neuromast location circled in red), *Tg(mpeg1:GFP)* macrophage recruitment, and *slc7a7* ISH signal at 0 h (C–C″), 2 h (D–D″) and 4 h (E–E″) after exposure to $CuSO_4$. Close-up observation of neuromast L4 at 2 hpt shows that *slc7a7* is expressed by macrophages recruited at the damaged neuromast (F,G). Scale bars: 50 µm.

DISCUSSION

In this study, we have found that Slc7a7-deficient zebrafish lack microglia because Slc7a7 is vital for tissue macrophages with sustained efferocytic activity. Thus, macrophages that have entered the brain and retina to become microglia start to die when the main wave of neuronal DCD occurs, triggering intense efferocytic work from these macrophages to eliminate the numerous neuron corpses. In the OT – the most routinely documented brain compartment in zebrafish microglia studies – the initial entry of Slc7A7-deficient macrophages can be easily overlooked because the main developmental influx of macrophages into the OT is triggered by signals emanating from the dying neurons (Xu et al., 2016). Therefore, when the neuronal DCD wave begins by 2.5 dpf, the attracted macrophages immediately have to engulf many neuron corpses, and die right away if they are Slc7a7-deficient. In support of this scenario, we had initially noticed that the few NR-labeled microglial spots found in the mutant OT, usually together with signs of microglial demise, often occurred in the ventrolateral corners of the OT (hence the name *cerise* that we gave to this mutant). A recent study precisely showed that these are indeed the main sites of macrophage entry into the OT (Xu et al., 2016). In contrast, in the retina, the macrophage/microglia number has already reached its plateau by 2 dpf (Herbomel et al., 2001; Demy et al., 2017); therefore in Slc7a7-deficient embryos, the demise of this already established population when the neuronal DCD begins is much more evident than in the OT.

In both the OT and the retina, we found a substantial infiltration of neutrophils following the demise of macrophages/microglia there. This neutrophil infiltration cannot be merely due to the accumulation of neuronal corpses in the absence of microglia to engulf them, since it does not occur in other microglia-deficient mutants such as the CSF1R-deficient *panther* (Herbomel et al., 2001; Wu et al., 2018). It is most likely due to signals emanating from the dying microglia itself, because these infiltrating neutrophils do interact with the dying microglia, and up to 9 dpf we found them only when and wherever dying/dead microglial cells were present. A similar neutrophil infiltration has been previously reported in one particular mutant, deficient in Nlrc3l (Shiau et al., 2013), in which macrophages showed an early inflammatory phenotype, with a clear induction of *il1-β* and *cxcl8*. In contrast, we found no induction of these cytokine genes in *cerise* embryos *in toto*, nor any sign of *il1-β* induction in Slc7a7-deficient macrophages *in situ* using a Tg(il1-β:GFP) reporter line (Nguyen-Chi et al., 2014). Hence, the molecular signals attracting neutrophils to the dying microglia in the CNS remain to be identified.

Since our initial characterization of zebrafish primitive microglia (Herbomel et al., 2001), its intense vital staining by NR has been widely used as an easy readout for microglia number, notably in forward and reverse genetic screens (Kuil et al., 2019 and references therein). Here, we clarify that this strong NR staining actually reflects the specific accumulation of NR over time in the already

acidified phagosomes containing apoptotic bodies. Therefore beyond microglia, it is a very convenient live staining method to spot any episode of high efferocytic activity among the various tissue macrophage populations of the developing fish. We have thus identified two such episodes, and the correlative demise of the corresponding macrophage populations in the *cerise* mutant – (i) the engulfment by 3 dpf of the hatching gland cells that died following the release by apocrine secretion of their protease-loaded granules into the medium to trigger hatching, and (ii) the engulfment of many primitive erythrocytes once the definitive ones are produced, peaking from 5–6 dpf onwards. These examples further indicate that Slc7a7 is vital not specifically for microglia but for all tissue macrophages that undergo a phase of high efferocytic activity. This can also readily explain our observation that by 48 hpf, that is, before the above three prominent developmental apoptosis events, mutant embryos already have 10% less macrophages overall, and 25% less macrophages in the retina than their non-mutant siblings. Indeed, before 48 hpf, macrophages do have to engulf corpses resulting from more limited developmental apoptosis events; for example, among the pro-erythroblasts by the onset of blood circulation (Herbomel et al., 1999), among the newly born neurons of cranial ganglia by 30–35 hpf (Herbomel et al., 2001) and within the still neuroepithelial retina by 36 hpf (Cole and Ross, 2001).

We also found that *slc7a7* expression is induced in efferocytic macrophages *in vivo*, and our assay of macrophage recruitment to chemically damaged neuromasts showed that *slc7a7* induction occurs within 1–2 h following macrophage contact with apoptotic cells, and is over by 2 h later. For macrophage populations whose efferocytic activity is sustained over many hours, or days (as for the primitive microglia), *slc7a7* expression becomes continually stimulated accordingly. It is conceivable that such continual stimulation may eventually turn into a stable expression feature of such a tissue macrophage population, even once their sustained efferocytic activity has subsided. We note indeed that, in comparative transcriptome studies, *slc7a7* was found expressed at a high level in adult zebrafish microglia relative to brain tissue (Oosterhof et al., 2017), and in adult mouse microglia relative to peritoneal macrophages (Hickman et al., 2013). Interestingly, we found a developmental expression pattern very similar to *slc7a7* for at least two other genes, coding for lysosomal proteins involved in protein and lipid catabolism, cathepsin B and prosaposin (P.H., unpublished data), that then also remained highly expressed in adult microglia (Oosterhof et al., 2017). This suggests that a whole subset of microglial markers or traits may well be acquired through – and thus be dependent on – an episode of high and sustained efferocytic activity, namely the main neuronal DCD wave.

Thus our conclusion is quite different from that of Rossi et al. (2015) who claimed that *slc7a7* expression identifies microglial precursors prior to their entry into the brain. This conclusion was drawn from an embryo-wide photoconversion at 24 hpf of Kaede protein expressed from a transgenic *slc7a7* locus; at 4 dpf they found photoconverted Kaede in microglial cells. However, the photoconverted Kaede in the microglial cells at 4 dpf appeared to delineate not the entire cells but an intracellular compartment – most likely phagolysosomal (see figure 4P–R in Rossi et al., 2015), and the approximately four *slc7a7*+ macrophages that can be detected by 24 hpf (see figure 3K in Rossi et al., 2015) could hardly account for the amount of photoconverted Kaede seen in most or all microglial cells at 4 dpf (see figure 4N in Rossi et al., 2015). Our own interpretation of these data is that, owing to the high diffuse *slc7a7* expression seen throughout the head at 24 hpf (see figure 3I in Rossi et al., 2015), the global photoconversion performed at 24 hpf notably photoconverted Kaede throughout the brain (see figure 4K,N in Rossi et al., 2015), and this photoconverted Kaede accumulated in the phagolysosomal compartment of the microglial cells when the latter massively engulfed dead neurons during the neuronal DCD wave.

Why is Slc7a7 vital for highly efferocytic macrophages? Sustained efferocytosis requires macrophages to catabolize the content of numerous cell corpses at a high rate, and then recycle or expel the resulting metabolites. These challenges involve adaptations of the macrophage metabolism that are only beginning to be uncovered (Han and Ravichandran, 2011). Since Slc7a7 is the main cationic amino acid transporter expressed in the macrophages, and is known to act mainly as an exporter (Fotiadis et al., 2013), Slc7a7 deficiency would predictably lead to a large excess of cationic amino acids in efferocytic macrophages. An excess of arginine could conceivably be detrimental to the cell if it is used to produce excess NO via NO synthases (NOSs); however, we found that zebrafish primitive macrophages do not express any of the *nos* genes (Table S1). Hence, the basis of a potential toxicity of excess intracellular cationic amino acids for the macrophage remains to be identified.

In humans, inborn SLC7A7 deficiency causes a disease named lysinuric protein intolerance (LPI) (Torrents et al., 1999), the primary symptoms of which are due to the absence of SLC7A7 in the basolateral membrane of gut enterocytes (where it normally allows the transfer of dietary cationic amino acids from the gut to the blood) and kidney tubules (where it allows reabsorption of cationic amino acids). However, beside these common symptoms, LPI patients suffer from variable, quite diverse types of all too often fatal symptoms, at least two of which suggest an involvement of macrophages – pulmonary alveolar proteinosis and hemophagocytic lymphohistiocytosis (Mauhin et al., 2017; Ogier de Baulny et al., 2012). It has been very difficult to study the etiology of these symptoms due the lack of a viable mouse model until very recently (Bodoy et al., 2019). In addition to the symptoms listed above, a recent update of LPI patients' follow-up pointed that over half of the patients presented with cognitive disorders (Mauhin et al., 2017). This has been explained so far by chronic or episodic hyperammonemia (due to a urea cycle disorder consequent to low serum arginine). Our study suggests an alternative or additional possible cause. As nothing is known about microglia in LPI patients, it is conceivable that as in the zebrafish, the first wave of microglia die *in utero* during the developmental neuronal death episodes, and that their demise contributes to later cognitive disorders.

MATERIALS AND METHODS

Zebrafish lines and embryos

Wild-type (WT), transgenic and mutant zebrafish embryos were raised at 28°C in embryo water [Volvic® water containing 0.28 mg/ml Methylene Blue (M-4159; Sigma) and 0.03 mg/ml 1-phenyl-2-thiourea (P-7629; Sigma)], and were staged according to Westerfield (1993).

AB and Tübingen WT fish (ZIRC), and the transgenic lines *Tg(mfap4:mCherry-F)*^{ump6} (Phan et al., 2018), *Tg(mpeg1:Gal4FF)*^{gl25} (Palha et al., 2013), *Tg(UAS:Kaede)rk8* (Hatta et al., 2006), *Tg(mpeg1:mCherry-F)*^{ump2} (Nguyen-Chi et al., 2014), *Tg(UAS-E1b:Eco.NfsB-mCherry)*^{c264} (Davison et al., 2007), *Tg(elavl3:EGFP)*^{knu3} (Park et al., 2000), *Tg(mpx:GFP)*^{i114} (Renshaw et al., 2006), *Tg(gata1:dsRed)*^{sd2} (Traver et al., 2003), *Tg(mpeg:GFP-CAAX)*^{sh425} (Keatinge et al., 2015), *Tg(lyz:DsRed2)*^{nz50} (Hall et al., 2007) have been used in this study. The *cerise*^{NO067} mutant was obtained by ENU chemical mutagenesis on a Tübingen WT background, and maintained by outcross of heterozygous carriers with WT/Tg fish. The fish were housed in the Institut Pasteur fish facilities accredited by the French Ministry of Agriculture. Work on fish was performed in compliance with French and European regulations on care and protection of laboratory animals (EC

Directive 2010/63, French Law 2013-118, February 6th, 2013). All experiments performed on >5 dpf larvae were approved by the Ethics Committee #89 (CETEA Institut Pasteur) and registered under the reference DAP190108.

Mapping and identification of the mutation

1500 *cerise* homozygous mutant larvae were collected along with a few of their siblings after NR-based screening at 4 dpf. We first mapped the mutation to a 7.7 Mb interval on linkage group 7 (LG7) by bulk segregant analysis of SSLP markers, as described previously (Geisler et al., 2007). Then whole-genome Illumina HiSeq2000 sequencing (Leshchiner et al., 2012) of 20 siblings and 220 mutants followed by SNP analysis led to the identification of a mutation within this region, a AG>TG change at the splice acceptor of *slc7a7* intron 4 (GenBank: BC110115.1). To confirm the mis-splicing induced by the *cerise* mutation, total RNA was isolated with Trizol reagent (Invitrogen, 15596-026) according to manufacturer's instructions, and retrotranscribed into cDNA by M-MLV reverse transcriptase (Invitrogen, 28025-013). A PCR was performed to amplify the full mutant *slc7a7* cDNA using: forward primer 5′-AAATAACATGACCTG-CCCGC-3′ and reverse primer 3′-AATCCCGTCAGCAGCTTTTG-5′.

The 2395 bp amplicon was then fully sequenced (Eurofins Genomics) using: sequencing primer 1, 5′-TGTGACCACGACAATGAACG-3′; sequencing primer 2, 5′-TCGCTGGTAGTGTGGACAAT-3′; sequencing primer 3, 5′-ATCATCACTGGCCTGGTCAA-3′; and sequencing primer 4, 5′-TGCTTCAAGGCTGTTCTTCG-3′.

The result was that exon 5 was skipped and exon 4 spliced to exon 6; the rest of the mRNA was as predicted for WT.

Morpholino injections

Two splice blocking antisense morpholinos (Mos) against *slc7a7* RNA were synthesized by Gene Tools: Sp22 (targeting the exon2/intron2 donor site), 5′-ATACATCCAACTCACAGATGCAGGC-3′, and Sp55 (targeting the exon5/intron5 donor site), 5′-AAAGTGTTTATTACTCACCACAGCC-3′. 1–5 nl of 0.6 mM Mo solution was microinjected in 1-cell–2-cell-stage embryos.

Neutral Red vital staining of microglia and Sudan Black staining of neutrophils

Highly efferocytic cells, including microglia, were revealed in live embryos and larvae by adding NR [N-4638; Sigma] to Volvic water at a final concentration of 5 µg/ml for 2 h, or 2.5 µg/ml for ∼5 h when an optimal signal-to-noise ratio was desired. After incubation in the dark at 28°C, larvae were rinsed in Volvic water, anesthetized and observed under a stereomicroscope or a compound wide-field microscope (see below). Sudan Black staining of neutrophils in formaldehyde-fixed embryos was undertaken as previously described (Le Guyader et al., 2008).

Neuromast damage with $CuSO_4$

Neuromast hair cell damage was achieved by incubating 54 hpf larvae in 50 µM $CuSO_4$ (1.02791; Sigma) for 30 min, as previously described (Olivari et al., 2008). Treated larvae were then rinsed three times with embryo water. After WISH, the *slc7a7* RNA signal was manually assessed for each neuromast (SO1-L7) using a Macrofluo microscope (Leica), and/or imaged on a Reichert Polyvar2 wide-field microscope (see below).

Ablation of erythrocytes with PHZ

On the day of the experiment, phenylhydrazine (PHZ; P26252; Sigma) was dissolved in water at a concentration of 5 mg/ml for stock solution. Dechorionated live embryos at 30–35 hpf were then soaked in 5 µg/ml PHZ in embryo water overnight in the dark so as to induce massive death of primitive erythrocytes (Pelster and Burggren, 1996). The embryos were washed the next day with Volvic© water and processed for further experiments.

Whole-mount mRNA *in situ* hybridization and immunohistochemistry

Embryos and larvae were anesthetized with 0.16 mg/ml tricaine (A-5040; Sigma) at the stage of interest, then fixed overnight at 4°C in 4% methanol-free formaldehyde (Polysciences, Cat# 040181). Whole-mount *in situ* hybridization (WISH) was performed according to Thisse and Thisse (2004). Whole-mount immunohistochemistry (WIHC) was performed as described previously (Murayama et al., 2006), omitting the acetone treatment. The primary antibodies used were: rabbit anti-zebrafish L-plastin and PU.1 polyclonal antibodies (at 1:5000 and 1:800 dilution, respectively) (Le Guyader et al., 2008). The secondary antibodies were Cy3-coupled anti-rabbit-IgG antibody [111-166-003; Jackson Immunoresearch) at 1:800 dilution, Cy3-coupled anti-mouse-IgG antibody (115-166-003; Jackson Immunoresearch) at 1:500 dilution, and Alexa Fluor 488-coupled anti-rabbit-IgG antibody (A11070; Molecular Probes) at 1:500 dilution.

SNP genotyping of fixed embryos

After WISH or WIHC and counting of macrophages/microglial cells in a clutch of *cerise* and sibling embryos, the tail tip of each embryo was cut using a sharp scalpel and isolated in a PCR tube for genotyping. Genomic DNA was extracted by boiling at 90°C for 30 min in 40 µl of extraction buffer (25 mM NaOH, 0.2 mM EDTA), then the pH was neutralized by adding Tris-HCl. Genotyping was performed by qPCR using forward primers ending at and including the *cerise* mutation: WT-complementary forward primer, 5′-CCCTCTGGTGGTTATTTTTTCA-3′, mutant-complementary forward primer 5′-CCCTCTGGTGGTTATTTTTTCT-3′. The reverse primer 5′-CCACAGCATCACTGTCCAG-3′ was designed so as to generate a 142 nt amplicon, optimal for qPCR reaction. qRT-PCR was performed using Takyon Rox SYBR Master mix blue dTTP kit (Eurogentec, Cat#: UF-RSMT-B0701), and carried out for three biological replicates with measurements taken from three technical replicates on an Applied Biosystems 7300 Real Time PCR system (Thermo Fisher). Mutants and siblings were then sorted by comparing their amplification curves upon qPCR with the WT and mutant set of primers (Ct_{mutant}–Ct_{WT}).

Microscopy and image analysis

Low-magnification bright-field images were acquired using video cameras mounted on a Leica Macrofluo microscope driven by the Metavue (Metamorph) software or a Zeiss Macrofluo microscope driven by the Zen software (Zeiss).

Wide-field video-enhanced (VE) Nomarski/differential interference contrast (DIC) and fluorescence microscopy were performed as described previously (Herbomel and Levraud, 2005; Murayama et al., 2006), through the 40×/1.00 NA water-immersion objective of a Nikon 90i microscope and the 40×/1.00 NA oil-immersion objective of a Reichert Polyvar 2 microscope. Images were obtained from a HV-D20 3-CCD camera (Hitachi) and digitized through a GVD-1000 DV tape recorder (Sony); then still images were collected using the BTVpro software (Bensoftware, London).

For fluorescence confocal imaging, embryos and larvae were mounted as previously described (Demy et al., 2017). Images were then captured at selected times on an inverted Leica SP8 set-up allowing multiple point acquisition, so as to image mutants and their siblings in parallel. Image stacks were processed with the LAS software to generate maximum intensity projections, or were exported into the Photoshop (Adobe) or Imaris software (Bitplane) for further analyses.

RNA-seq analysis of macrophages in zebrafish larvae

Zebrafish larvae from three different transgenic backgrounds highlighting macrophages – *Tg(mpeg1:mCherry)*, *Tg(mpeg1:Gal4; UAS:NfsB-mCherry)*, and *Tg(mpeg1:mCherry; mpx:gfp)* – were anesthetized at 3 dpf with tricaine, then dissociated into single-cell suspensions as previously described (Covassin et al., 2006). The red fluorescent macrophages were sorted by FACS, collected directly in lysis buffer, and RNA was extracted using a miRNeasy Micro kit (217084; Qiagen). Sequencing was performed on Illumina HiSeq2500 by ZF-Screens (Leiden, Netherlands) on three biological replicates: Tg(mpeg1:mCherry) (RNA extracted from 9480 cells of 92 embryos), Tg(mpeg1:Gal4/UAS:NfsB-mCherry) (RNA extracted from 10,875 cells of 146 embryos), amd Tg(mpeg1:mCherry/mpx:gfp) (RNA extracted from 10,004 cells of 196 embryos). 10 Mreads of 50 nt (0.5 Gb) were obtained for each replicate. The resulting data were analyzed with the DESeq software.

Statistical analysis

Statistical analyses and graphic representations were undertaken using Prism software. Distributions were normalized by log, and an analysis of variance (two-way ANOVA) was performed. qPCR samples were analyzed using the ΔΔCt method; the mean Ct value of housekeeping gene *ef1a* was used for normalization; the 2ΔΔCt values were graphed with the geometric mean±s.e.m. to estimate the fold change.

Acknowledgements

We wish to thank N. Trede and all members of the Trede lab for hosting and guiding D. L. Demy for the initial mapping of the *cerise* mutation, J.-P. Levraud for providing methods and material for mutant genotyping and cDNA sequencing, and our fish facility team for their excellent care of the fish.

Competing interests

The authors declare no competing or financial interests.

Author contributions

Conceptualization: D.L.D., R.N., M.T., P.H.; Methodology: D.L.D., M.C., R.N., M.T., I.L., W.G., P.H.; Software: I.L., W.G.; Validation: D.L.D., M.C., R.N., M.T., I.L., W.G., P.H.; Formal analysis: D.L.D., R.N., M.C., M.T., I.L., P.H.; Investigation: D.L.D., M.C., R.N., M.T., M.L.B., C.B., I.L., P.H.; Resources: D.L.D., M.T., I.L., W.G., P.H.; Data curation: D.L.D., P.H.; Writing - original draft: D.L.D., P.H.; Writing - review & editing: D.L.D., P.H.; Visualization: D.L.D., M.C., R.N., M.T., M.L.B., P.H.; Supervision: P.H.; Project administration: P.H.; Funding acquisition: P.H.

Funding

This work was supported by grants to P.H. from the European Commission through the FP6 'ZF-Models' Integrated Project, from the Fondation pour la Recherche Médicale ('FRM 2012 team' #DEQ20120323714, 'FRM 2016 team' #DEQ20160334881) and from the Agence Nationale de la Recherche Laboratoire d'Excellence Revive (Investissement d'Avenir; ANR-10-LABX-73).

Supplementary information

Supplementary information available online at
https://jcs.biologists.org/lookup/doi/10.1242/jcs.249037.supplemental

Peer review history

The peer review history is available online at
https://jcs.biologists.org/lookup/doi/10.1242/jcs.249037.reviewer-comments.pdf

References

Bodoy, S., Sotillo, F., Espino-Guarch, M., Sperandeo, M. P., Ormazabal, A., Zorzano, A., Sebastio, G., Artuch, R. and Palacín, M. (2019). Inducible slc7a7 knockout mouse model recapitulates lysinuric protein intolerance disease. *Int. J. Mol. Sci.* **20**, 5294. doi:10.3390/ijms20215294

Carrillo, S. A., Anguita-Salinas, C., Peña, O. A., Morales, R. A., Muñoz-Sánchez, S., Muñoz-Montecinos, C., Paredes-Zúñiga, S., Tapia, K. and Allende, M. L. (2016). Macrophage recruitment contributes to regeneration of mechanosensory hair cells in the zebrafish lateral line. *J. Cell. Biochem.* **117**, 1880-1889. doi:10.1002/jcb.25487

Cole, L. K. and Ross, L. S. (2001). Apoptosis in the developing zebrafish embryo. *Dev. Biol.* **240**, 123-142. doi:10.1006/dbio.2001.0432

Covassin, L., Amigo, J. D., Suzuki, K., Teplyuk, V., Straubhaar, J. and Lawson, N. D. (2006). Global analysis of hematopoietic and vascular endothelial gene expression by tissue specific microarray profiling in zebrafish. *Dev. Biol.* **299**, 551-562. doi:10.1016/j.ydbio.2006.08.020

Davison, J. M., Akitake, C. M., Goll, M. G., Rhee, J. M., Gosse, N., Baier, H., Halpern, M. E., Leach, S. D. and Parsons, M. J. (2007). Transactivation from Gal4-VP16 transgenic insertions for tissue-specific cell labeling and ablation in zebrafish. *Dev. Biol.* **304**, 811-824. doi:10.1016/j.ydbio.2007.01.033

Demy, D. L., Tauzin, M., Lancino, M., Le Cabec, V., Redd, M., Murayama, E., Maridonneau-Parini, I., Trede, N. and Herbomel, P. (2017). Trim33 is essential for macrophage and neutrophil mobilization to developmental or inflammatory cues. *J. Cell Sci.* **130**, 2797-2807. doi:10.1242/jcs.203471

Ferri-Lagneau, K. F., Moshal, K. S., Grimes, M., Zahora, B., Lv, L., Sang, S. and Leung, T. C. (2012). Ginger stimulates hematopoiesis via Bmp pathway in Zebrafish. *PLoS ONE* **7**, e39327. doi:10.1371/journal.pone.0039327

Fotiadis, D., Kanai, Y. and Palacín, M. (2013). The SLC3 and SLC7 families of amino acid transporters. *Mol. Asp. Med.* **34**, 139-158. doi:10.1016/j.mam.2012.10.007

Geisler, R., Rauch, G.-J., Geiger-Rudolph, S., Albrecht, A., van Bebber, F., Berger, A., Busch-Nentwich, E., Dahm, R., Dekens, M. P. S., Dooley, C. et al. (2007). Large-scale mapping of mutations affecting zebrafish development. *BMC Genomics* **8**, 11. doi:10.1186/1471-2164-8-11

Hall, C., Flores, M. V., Storm, T., Crosier, K. and Crosier, P. (2007). The zebrafish lysozyme C promoter drives myeloid-specific expression in transgenic fish. *BMC Dev. Biol.* **7**, 42. doi:10.1186/1471-213X-7-42

Han, C. Z. and Ravichandran, K. S. (2011). Metabolic connections during apoptotic cell engulfment. *Cell* **147**, 1442-1445. doi:10.1016/j.cell.2011.12.006

Hatta, K., Tsujii, H. and Omura, T. (2006). Cell tracking using a photoconvertible fluorescent protein. *Nat. Protoc.* **1**, 960-967. doi:10.1038/nprot.2006.96

Herbomel, P. and Levraud, J.-P. (2005). Imaging early macrophage differentiation, migration and behaviours in live zebrafish embryos. *Methods Mol. Med.* **105**, 199-214. doi:10.1385/1-59259-826-9:199

Herbomel, P., Thisse, B. and Thisse, C. (1999). Ontogeny and behaviour of early macrophages in the zebrafish embryo. *Development* **126**, 3735-3745.

Herbomel, P., Thisse, B. and Thisse, C. (2001). Zebrafish early macrophages colonize cephalic mesenchyme and developing brain, retina, and epidermis through a M-CSF receptor-dependent invasive process. *Dev. Biol.* **238**, 274-288. doi:10.1006/dbio.2001.0393

Hickman, S. E., Kingery, N. D., Ohsumi, T. K., Borowsky, M. L., Wang, L.-C., Means, T. K. and El Khoury, J. (2013). The microglial sensome revealed by direct RNA sequencing. *Nat. Neurosci.* **16**, 1896-1905. doi:10.1038/nn.3554

Keatinge, M., Bui, H., Menke, A., Chen, Y.-C., Sokol, A. M., Bai, Q., Ellett, F., Da Costa, M., Burke, D., Gegg, M. et al. (2015). Glucocerebrosidase 1 deficient Danio rerio mirror key pathological aspects of human Gaucher disease and provide evidence of early microglial activation preceding alpha-synuclein-independent neuronal cell death. *Hum. Mol. Genet.* **24**, 6640-6652. doi:10.1093/hmg/ddv369

Kuil, L. E., Oosterhof, N., Geurts, S. N., Van Der Linde, H. C., Meijering, E. and Van Ham, T. J. (2019). Reverse genetic screen reveals that Il34 facilitates yolk sac macrophage distribution and seeding of the brain. *Dis. Model. Mech.* **12**, dmm037762. doi:10.1242/dmm.037762

Le Guyader, D., Redd, M. J., Colucci-Guyon, E., Murayama, E., Kissa, K., Briolat, V., Mordelet, E., Zapata, A., Shinomiya, H. and Herbomel, P. (2008). Origins and unconventional behavior of neutrophils in developing zebrafish. *Blood* **111**, 132-141. doi:10.1182/blood-2007-06-095398

Leshchiner, I., Alexa, K., Kelsey, P., Adzhubei, I., Austin-Tse, C. A., Cooney, J. D., Anderson, H., King, M. J., Stottmann, R. W., Garnaas, M. K. et al. (2012). Mutation mapping and identification by whole-genome sequencing. *Genome Res.* **22**, 1541-1548. doi:10.1101/gr.135541.111

Li, Y., Du, X.-F., Liu, C.-S., Wen, Z.-L. and Du, J.-L. (2012). Reciprocal regulation between resting microglial dynamics and neuronal activity in vivo. *Dev. Cell* **23**, 1189-1202. doi:10.1016/j.devcel.2012.10.027

Mauhin, W., Habarou, F., Gobin, S., Servais, A., Brassier, A., Grisel, C., Roda, C., Pinto, G., Moshous, D., Ghalim, F. et al. (2017). Update on lysinuric protein intolerance, a multi-faceted disease retrospective cohort analysis from birth to adulthood. *Orphanet J. Rare Dis.* **12**, 3. doi:10.1186/s13023-016-0550-8

Meireles, A. M., Shiau, C. E., Guenther, C. A., Sidik, H., Kingsley, D. M. and Talbot, W. S. (2014). The phosphate exporter xpr1b is required for differentiation of tissue-resident macrophages. *Cell Rep.* **8**, 1659-1667. doi:10.1016/j.celrep.2014.08.018

Murayama, E., Kissa, K., Zapata, A., Mordelet, E., Briolat, V., Lin, H.-F., Handin, R. I. and Herbomel, P. (2006). Tracing hematopoietic precursor migration to successive hematopoietic organs during zebrafish development. *Immunity* **25**, 963-975. doi:10.1016/j.immuni.2006.10.015

Nguyen-Chi, M., Phan, Q. T., Gonzalez, C., Dubremetz, J.-F., Levraud, J.-P. and Lutfalla, G. (2014). Transient infection of the zebrafish notochord with E. coli induces chronic inflammation. *Dis. Model. Mech.* **7**, 871-882. doi:10.1242/dmm.014498

Ogier de Baulny, H., Schiff, M. and Dionisi-Vici, C. (2012). Lysinuric protein intolerance (LPI): a multi organ disease by far more complex than a classic urea cycle disorder. *Mol. Genet. Metab.* **106**, 12-17. doi:10.1016/j.ymgme.2012.02.010

Okabe, Y. and Medzhitov, R. (2016). Tissue biology perspective on macrophages. *Nat. Immunol.* **17**, 9-17. doi:10.1038/ni.3320

Olivari, F. A., Hernández, P. P. and Allende, M. L. (2008). Acute copper exposure induces oxidative stress and cell death in lateral line hair cells of zebrafish larvae. *Brain Res.* **1244**, 1-12. doi:10.1016/j.brainres.2008.09.050

Oosterhof, N., Holtman, I. R., Kuil, L. E., van der Linde, H. C., Boddeke, E. W. G. M., Eggen, B. J. L. and van Ham, T. J. (2017). Identification of a conserved and acute neurodegeneration-specific microglial transcriptome in the zebrafish. *Glia* **65**, 138-149. doi:10.1002/glia.23083

Palha, N., Guivel-Benhassine, F., Briolat, V., Lutfalla, G., Sourisseau, M., Ellett, F., Wang, C.-H., Lieschke, G. J., Herbomel, P., Schwartz, O. et al. (2013). Real-time whole-body visualization of chikungunya virus infection and host interferon response in zebrafish. *PLoS Pathog.* **9**, e1003619. doi:10.1371/journal.ppat.1003619

Park, H.-C., Kim, C.-H., Bae, Y.-K., Yeo, S.-Y., Kim, S.-H., Hong, S.-K., Shin, J., Yoo, K.-W., Hibi, M., Hirano, T. et al. (2000). Analysis of upstream elements in the HuC promoter leads to the establishment of transgenic Zebrafish with fluorescent neurons. *Dev. Biol.* **227**, 279-293. doi:10.1006/dbio.2000.9898

Pelster, B. and Burggren, W. W. (1996). Disruption of hemoglobin oxygen transport does not impact oxygen-dependent physiological processes in developing

embryos of zebra fish (Danio rerio). *Circ. Res.* **79**, 358-362. doi:10.1161/01.RES.79.2.358

Perdiguero, E. G. and Geissmann, F. (2016). The development and maintenance of resident macrophages. *Nat. Immunol.* **17**, 2-8. doi:10.1038/ni.3341

Peri, F. and Nüsslein-Volhard, C. (2008). Live imaging of neuronal degradation by microglia reveals a role for v0-ATPase a1 in phagosomal fusion in vivo. *Cell* **133**, 916-927. doi:10.1016/j.cell.2008.04.037

Phan, Q. T., Sipka, T., Gonzalez, C., Levraud, J.-P., Lutfalla, G. and Nguyen-Chi, M. (2018). Neutrophils use superoxide to control bacterial infection at a distance. *PLoS Pathog.* **14**, e1007157. doi:10.1371/journal.ppat.1007157

Renshaw, S. A., Loynes, C. A., Trushell, D. M. I., Elworthy, S., Ingham, P. W. and Whyte, M. K. B. (2006). A transgenic zebrafish model of neutrophilic inflammation. *Blood* **108**, 3976-3978. doi:10.1182/blood-2006-05-024075

Rossi, F., Casano, A. M., Henke, K., Richter, K. and Peri, F. (2015). The SLC7A7 transporter identifies microglial precursors prior to entry into the brain. *Cell Rep.* **11**, 1008-1017. doi:10.1016/j.celrep.2015.04.028

Shafizadeh, E., Peterson, R. T. and Lin, S. (2004). Induction of reversible hemolytic anemia in living zebrafish using a novel small molecule. *Comp. Biochem. Physiol. C Toxicol. Pharmacol.* **138**, 245-249. doi:10.1016/j.cca.2004.05.003

Shiau, C. E., Monk, K. R., Joo, W. and Talbot, W. S. (2013). An anti-inflammatory nod-like receptor is required for microglia development. *Cell Rep.* **5**, 1342-1352. doi:10.1016/j.celrep.2013.11.004

Svahn, A. J., Graeber, M. B., Ellett, F., Lieschke, G. J., Rinkwitz, S., Bennett, M. R. and Becker, T. S. (2013). Development of ramified microglia from early macrophages in the zebrafish optic tectum. *Dev. Neurobiol.* **73**, 60-71. doi:10.1002/dneu.22039

Thisse, B. and Thisse, C. (2004). Fast release clones: a high throughput expression analysis. *ZFIN Direct Data Submission*. https://zfin.org/ZDB-PUB-040907-1

Torrents, D., Mykkänen, J., Pineda, M., Feliubadaló, L., Estévez, R., De Rafael, C., Sanjurjo, P., Zorzano, A., Nunes, V., Huoponen, K. et al. (1999). Identification of SLC7A7, encoding y+LAT-1, as the lysinuric protein intolerance gene. *Nat. Genet.* **21**, 293-296. doi:10.1038/6809

Traver, D., Paw, B. H., Poss, K. D., Penberthy, W. T., Lin, S. and Zon, L. I. (2003). Transplantation and in vivo imaging of multilineage engraftment in zebrafish bloodless mutants. *Nat. Immunol.* **4**, 1238-1246. doi:10.1038/ni1007

Vojtech, L. N., Scharping, N., Woodson, J. C. and Hansen, J. D. (2012). Roles of inflammatory caspases during processing of zebrafish interleukin-1β in Francisella noatunensis infection. *Infect. Immun.* **80**, 2878-2885. doi:10.1128/IAI.00543-12

Westerfield, M. (1993). *The zebrafish book: A guide for the laboratory use of zebrafish (Brachydanio rerio)*. University of Oregon Press, Eugene, OR.

Wu, S., Xue, R., Hassan, S., Nguyen, T. M. L., Wang, T., Pan, H., Xu, J., Liu, Q., Zhang, W. and Wen, Z. (2018). Il34-Csf1r pathway regulates the migration and colonization of microglial precursors. *Dev. Cell* **46**, 552-563.e4. doi:10.1016/j.devcel.2018.08.005

Xu, J., Wang, T., Wu, Y., Jin, W. and Wen, Z. (2016). Microglia colonization of developing zebrafish midbrain is promoted by apoptotic neuron and lysophosphatidylcholine. *Dev. Cell* **38**, 214-222. doi:10.1016/j.devcel.2016.06.018

Supplementary Figures

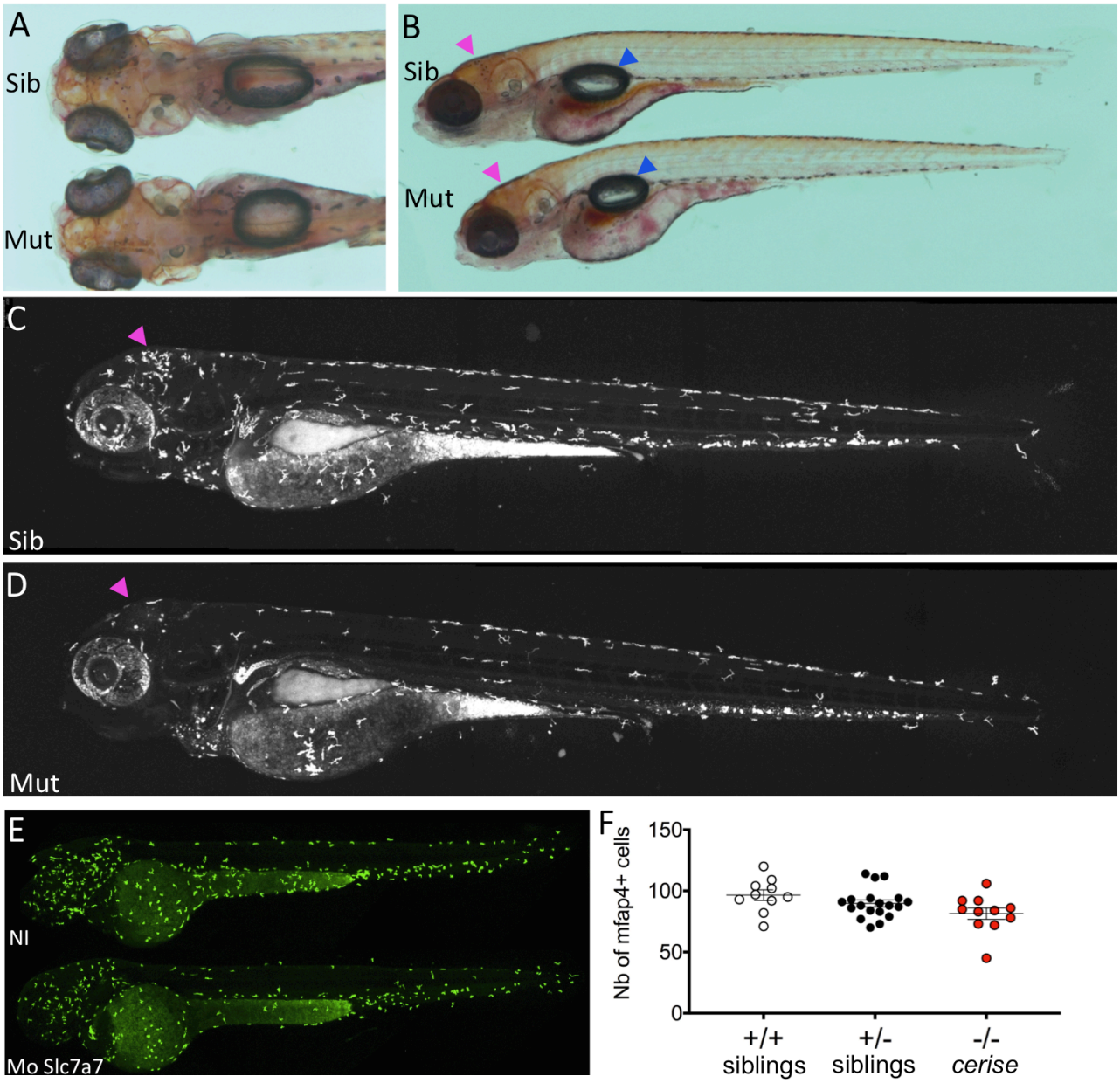

Fig. S1. Primitive macrophages are normally produced in Slc7a7 deficient zebrafish
(A-B) Dorsal **(A)** and lateral **(B)** view of a live *cerise* mutant and a sibling stained with Neutral Red at 5 dpf. The mutant, recognizable by its absence of microglia in the optic tectum (pink arrowheads), has overall normal morphology, with a well developed swimbladder (blue arrowheads).
(C-D) Lateral view of global macrophage population in live *Tg(mfap4:mCherryF)* control sibling **(C)** and cerise mutant **(D)** at 4 dpf.
(E) Lateral view of global macrophage population in live *Tg(mpeg:Gal4;UAS:Kaede)* control or slc7a7-sp22 morphant embryos at 48 hpf.
(F) Macrophage count in the whole body of 48 hpf *cerise* progeny according to their genotype, revealed by mfap4 ISH followed by qPCR genotyping. Error bars show mean±s.e.m.
Pink arrowheads point to tectal microglia. Sib, sibling; mut, mutant; NI, non-injected; Mo, morpholino; Nb, number

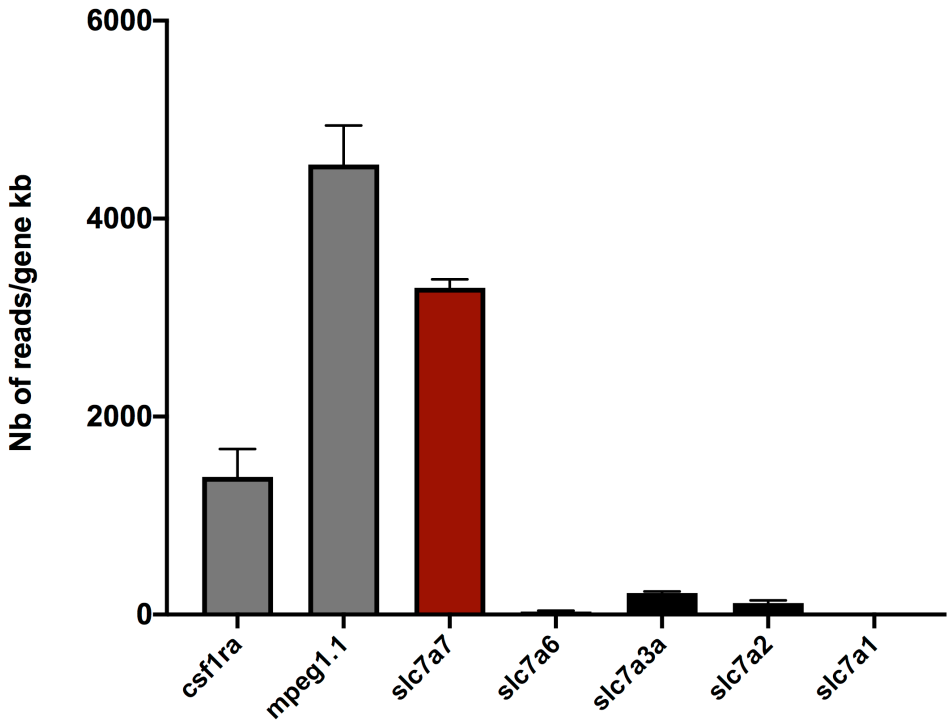

Fig. S2 : Slc7a7 is the most highly expressed cationic amino acid transporter in macrophages of zebrafish larvae at 3 dpf.

Macrophages were FACS-sorted from WT zebrafish larvae at 3 dpf, and subjected to RNAseq analysis (see M&M section). Expression levels are given here as number of reads per kilobase of mRNA sequence, for two typical macrophage-specific genes (*csfr1a* and *mpeg1.1*), and the 5 cationic amino acid transporters of the slc7 family. See also Table 1 for raw data and additional genes. Error bars show s.e.m.

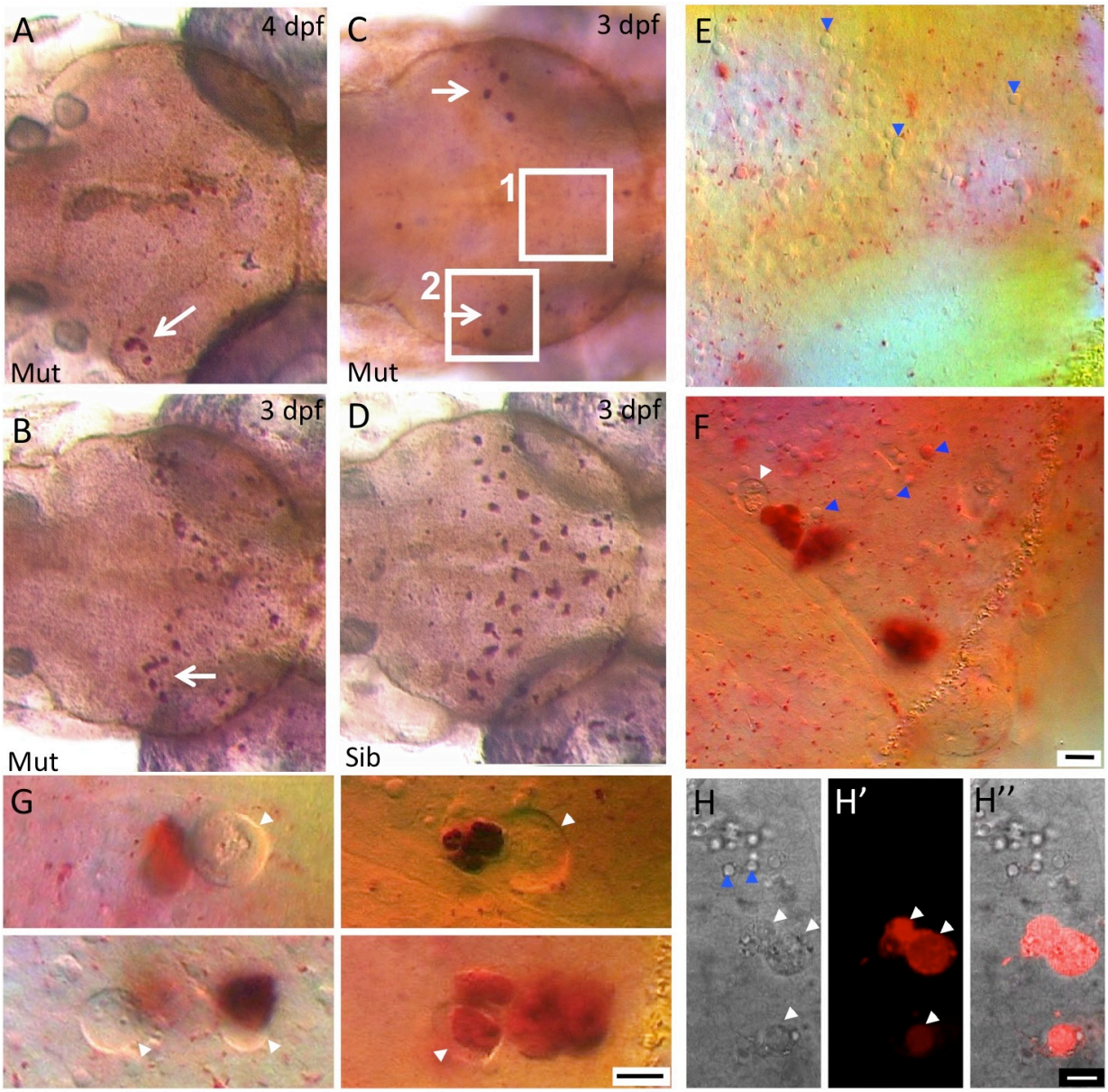

Fig. S3. Close examination of neutral red stained *cerise* mutant larvae suggest that primitive macrophages are able to initiate brain colonization, but die soon thereafter.
(A-F) Dorsal view, rostral to the right, of the optic tectum of live zebrafish larvae stained with Neutral Red; *cerise* mutants at 4 dpf **(A)** and 3 dpf **(B, C)**, sibling at 3 dpf **(D)**, and close-ups on the mutant NR+ material at 3 dpf **(E, F)** on regions shown by white frames in (C), and at still higher magnification in G. **(H-H'')** Close-up on tectal microglia in live *Tg[mfap4:mCherryF] cerise* mutant larvae at 3 dpf.
Blue arrowheads point to neuronal apoptotic bodies; white arrowheads point to abnormal large vacuoles (note that the DIC shadow cast contrast delineating their contour is inverted relative to that shown by the apoptotic bodies, indicating a lower refraction index, i.e. a less dense / more aqueous content) only in the mutant, always next to or including NR+ material. Scale bar, 10 µm. Sib, sibling; mut, mutant.

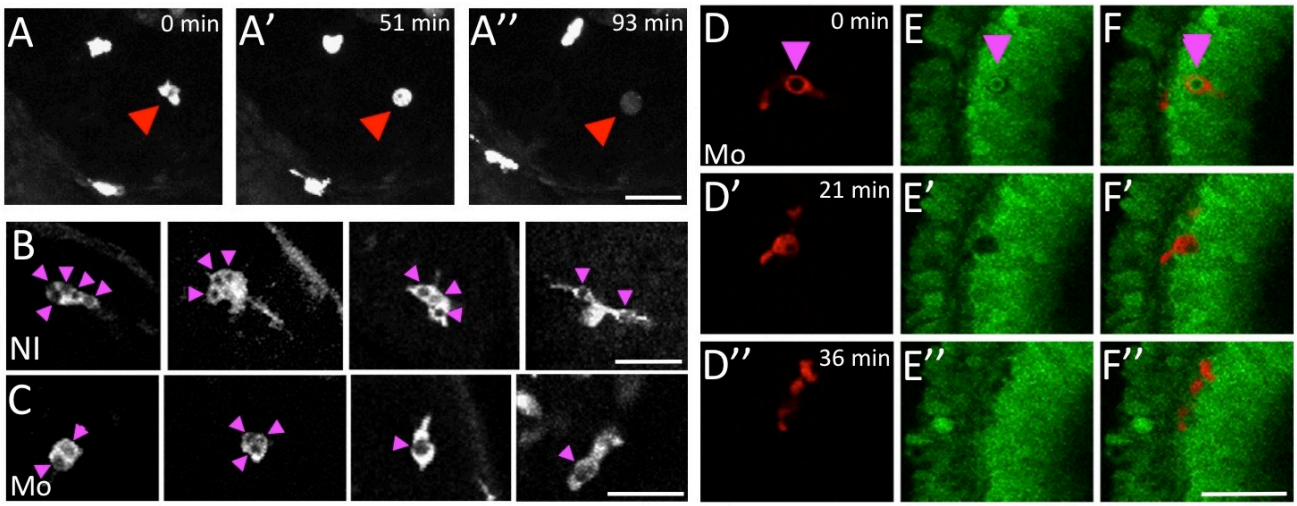

Fig. S4. The death of microglia in *cerise* correlates with their efferocytic activity

(A-A'') Close-ups on a dying mCherry+ macrophage in the retina of a 2.5 dpf *Tg(mpeg:Gal4; UAS:NfsB:mCherry)* slc7a7-sp22 morphant over time. See also Movie 2.

(B, C) Close-ups on mCherry+ macrophages in the optic tectum of live *Tg(mpeg1:Gal4; UAS:NfsB-mCherry)* control (B) or slc7a7-sp22 morphant (C) larvae at 3 dpf.

(D-F'') Close-ups on an apoptotic HuC:GFP+ neuron (E-E'') being engulfed by a mpeg1:mCherry+ macrophage which then dies (D-D''; F-F''), in the retina of a sp22 morphant over time.

Scale bars, 30 µm. Pink arrowheads point to phagosomes inside macrophages and red arrowheads to dying macrophages. NI, non-injected; Mo, morphant

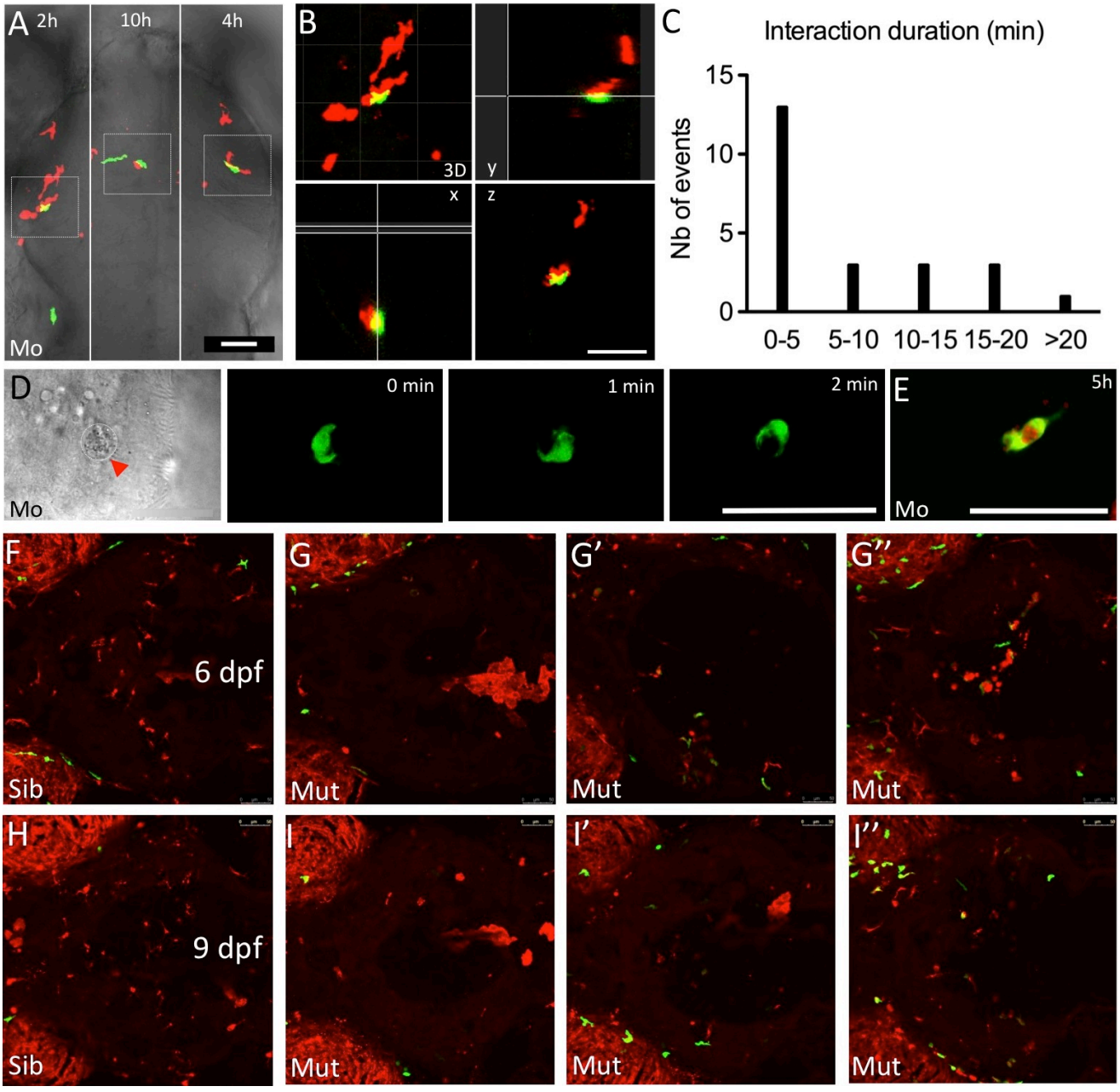

Fig. S5. Neutrophil - macrophage/microglia interactions in the brain of *cerise* mutants

(A, B, D, E) Selected time points and image sub-fields of *in vivo* time-lapse confocal imaging sequences of mpeg:1mCherry+ macrophages/microglia and mpx:GFP+ neutrophils in the OT of a slc7a7-sp22 morphant (A, B) or *cerise* mutant (D, E) at 3 dpf in dorsal view. (A) shows the whole OT, rostral to the top, divided in three subfields (left, central, right) to display microglia / neutrophil interactions that occurred at different time points in each sub-field. (B) Close-up and orthogonal views of the interaction shown in the left sub-field (t=2h) in (A). (C) Distribution of the macrophage/neutrophil interaction durations. (D, E) Longer interactions observed in morphant larvae displaying only a few macrophage/microglia remnants in the tectum; (D) a neutrophil rapidly moving around a macrophage remnant and sticking to it for hours; (E) a neutrophil that engulfed mCherry+ material, presumably from a macrophage. Scale bars, 50 µm

(F-I') Dorsal views, rostral to the left, of the OT of a sibling (F,H) and three different mutants (G-G''; I-I'') at 6 and 9 dpf in *Tg(mpeg1:mcherry; mpx:gfp)* background, showing macrophages in red and neutrophils in green. Neutrophils are rarer in the mutant OT than at 3 and 4 dpf, and whenever present, they correlate with the presence of dying microglia.

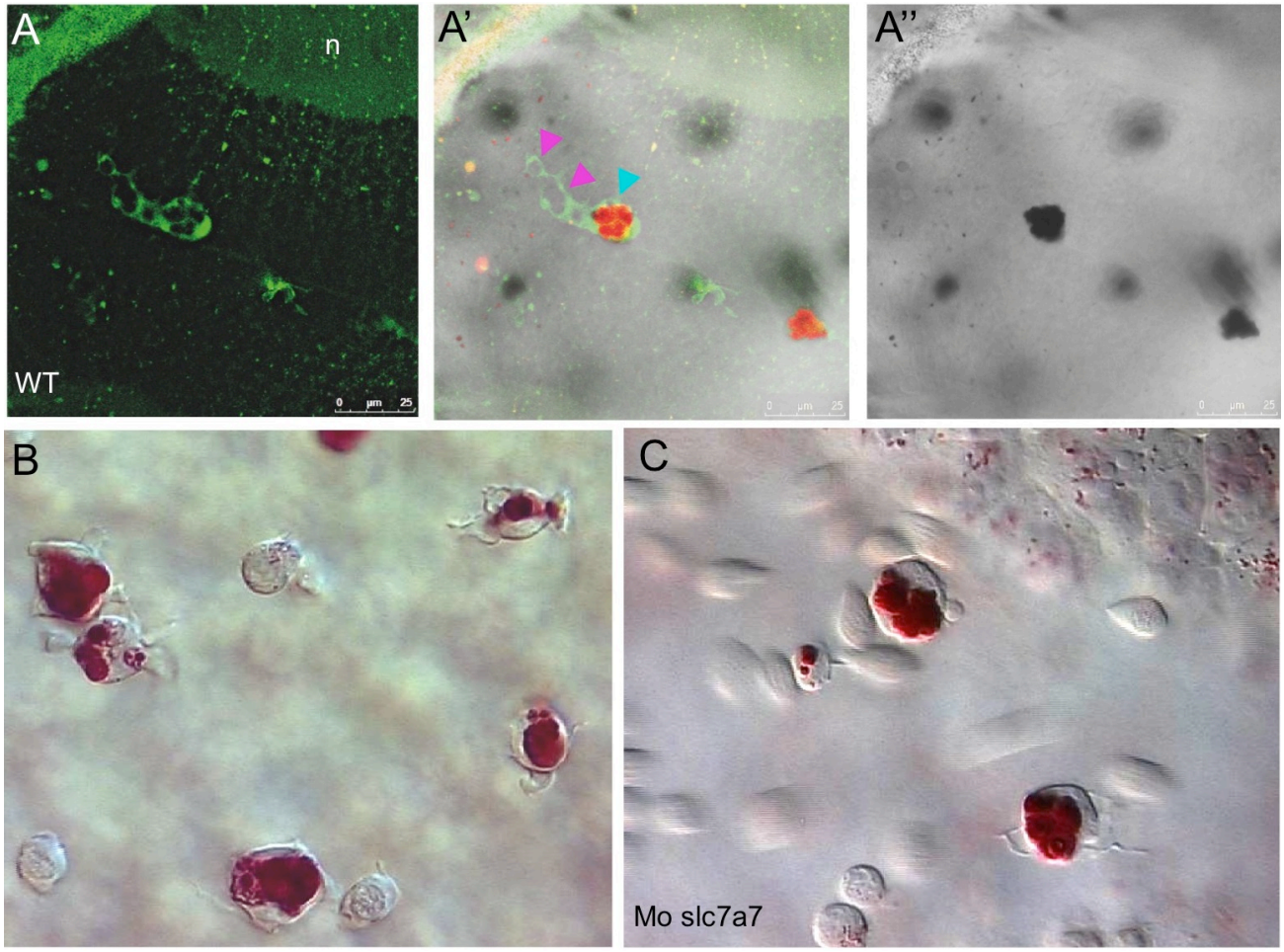

Fig. S6. Vital staining of zebrafish macrophages with Neutral Red highlights their acidified effero-phagosomes.

(A-A'') Close-up on two mpeg1:GFP+ tectal microglial cells after Neutral Red vital staining at 4 dpf; (A), confocal fluorescence image; (A'), fluorescence + brigh-field transmitted light image; (A''), bright-field only; n, neuropile; Neutral Red accumulates in the already acidified effero-phagosomes (blue arrowhead), whereas more recent efferophagosomes are NR-negative (pink arrowheads).

(B,C) VE-DIC/Nomarski observation in the yolk sac circulation valley (duct of Cuvier) of Neutral Red stained WT **(B)** and slc7a7 morphant **(C)** embryos at 30 hpf. Neutral Red accumulates in the effero-phagosomes containing engulfed apoptotic pro-erythroblasts. Macrophages in slc7a7 morphants are as efferocytic towards apoptotic pro-erythroblasts as in control embryos.

Table S1. Gene expression levels of Slc7 family members and arginine-dependent enzymes in macrophages of zebrafish larvae at 3 dpf.
Fluorescent macrophages were sorted from three different batches (replicates) of 3 dpf transgenic larvae (see M. & M.) and submitted to RNAseq analysis.
10 Mreads of 50 nt (0.5 Gb) were obtained for each replicate. The gene expression level is expressed in Number of reads per kilobase of RNA transcript.

Gene ID	Length (nt)	Gene Name	WikiGene Description	Nb of reads Sample 1	Nb of reads Sample 2	Nb of reads Sample 3	Mean nb reads	Nb reads/kb
Macrophage-specific genes								
ENSDARG00000007889	3365	csf1ra	colony stimulating factor 1 receptor, a	5423	2806	5819	4683	1392
ENSDARG00000090783	1150	mfap4	microfibrillar-associated protein 4	16987	25106	18724	20272	17628
ENSDARG00000055290	2634	mpeg1.1	macrophage expressed 1, tandem duplicate 1	13506	9986	12429	11974	4546
ENSDARG00000043093	2638	mpeg1.2	macrophage expressed 1, tandem duplicate 2	10297	9678	10435	13779	5223
Cationic amino acid transporters								
ENSDARG00000055226	2395	slc7a7	solute carrier family 7 (cationic amino acid transporter, y+L system), member 7 = y+LAT-1 (S-S bridged to Slc3a2)	8321	7682	7709	7904	3300
ENSDARG00000054423	1938	slc7a6	solute carrier family 7 (cationic amino acid transporter, y+ L system), member 6 = y+LAT-2 (S-S bridged to Slc3a2)	91	28	55	58	29
ENSDARG00000016439	2223	slc7a1	solute carrier family 7 (cationic amino acid transporter, y+ system), member 1 = CAT-1	8	0	2	3	1
ENSDARG00000037097	3800	slc7a2	solute carrier family 7 (cationic amino acid transporter, y+ system), member 2 = CAT-2	583	251	497	333	88
ENSDARG00000020645	4519	slc7a3a	solute carrier family 7 (cationic amino acid transporter, y+ system), member 3a = CAT-3	1110	970	870	983	217
ENSDARG00000061566	1929	slc7a3b	solute carrier family 7 (cationic amino acid transporter, y+ system), member 3b = CAT-3	52	87	33	57	30
ENSDARG00000036427	2303	slc3a2a	solute carrier family 3, member 2a (aka 4F2hc, CD98hc); glycoprotein partner of several SLCs, incl. Slc7a7, Slc7a6	13671	13916	12569	13385	5812
ENSDARG00000037012	2028	slc3a2b	solute carrier family 3, member 2b (aka 4F2hc, CD98hc); glycoprotein partner of several SLCs, incl. Slc7a7, Slc7a6	2532	3477	2230	2746	1354
Candidate arginine dependent pathways in macrophages								
ENSDARG00000026925	4149	nos2a	nitric oxide synthase 2a, inducible	0	0	0	0	0
ENSDARG00000031976	3428	nos2b	nitric oxide synthase 2b, inducible	7	0	0	2	1
ENSDARG00000071703	1041	arg1	arginase-1	0	0	0	0	0
ENSDARG00000039269	2257	arg2	arginase-2	820	372	807	666	295

Movie 1 (related to Fig. 2A-C). Dynamics of primitive microglia in the midbrain optic tectum of WT zebrafish larva by 3 dpf. Time-lapse confocal imaging of a 3 dpf *Tg(mpeg1:gal4; uas:Nfsb-mCherry)* larva injected with a control morpholino at the 1-2 cell stage. Dorsal view, rostral to the top (maximum projection from a z-stack); time step = 3 min.

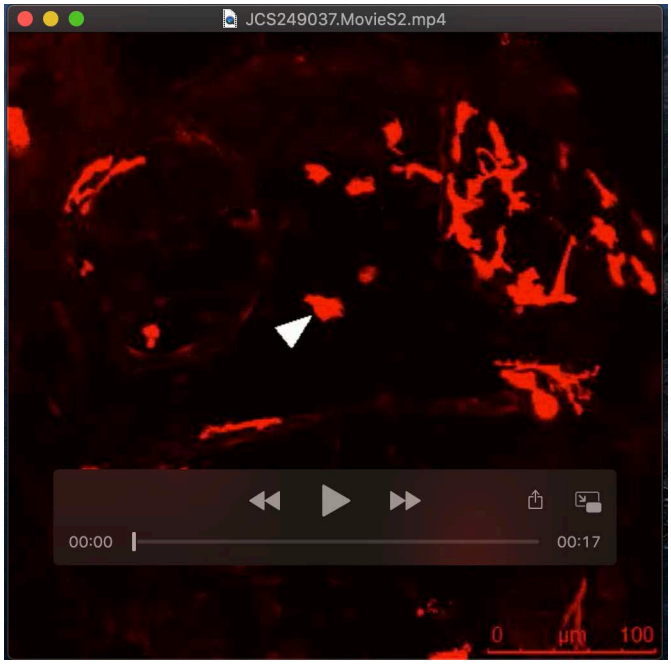

Movie 2 (related to Fig. 2A-C). Primitive microglial cells die in the midbrain optic tectum of a Slc7a7-deficient zebrafish larva by 3 dpf. Time-lapse confocal imaging of a 3 dpf *Tg(mpeg1:gal4; uas:Nfsb-mCherry)* larva injected with the slc7a7-sp22 morpholino at the 1-2 cell stage, and imaged in parallel with the control Mo-injected larva shown in Movie 1, within the same glass-bottomed dish. Dorsal view, rostral to the top (maximum projection from a z-stack); time step = 3 min. Selected time points of this movie are shown in Fig. 2C. The macrophages / microglial cells tracked by a white and a yellow arrowhead correspond to the dark and light green arrowheads in Fig. 2C, respectively. Another series of consecutive death/ engulfment/ death events occuring nearby in this movie is tracked by a blue/grey series of arrowheads in Fig. 2C. The z-stack used to produce the maximum projection shown here is somewhat thicker than in Fig. 2C, such that at the beginning, on the right side, it includes macrophages that are not within the brain but above it.

Journal of Cell Science • Supplementary information

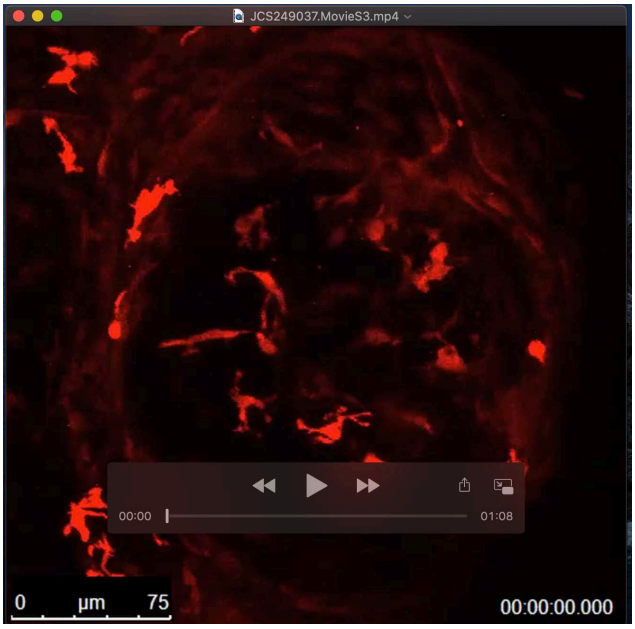

Movie 3 (related to fig. 2G-H'). Dynamics of primitive microglia in the retina of WT zebrafish larva from 2.5 dpf. Time-lapse confocal imaging starting by 54 hpf of a *Tg(mpeg1:gal4; uas:Nfsb-mCherry)* larva injected with a control morpholino at the 1-2 cell stage. Lateral view (maximum projection from a z-stack); time step = 3 min.

Movie 4 (related to fig. 2G-H'). Dynamics of primitive microglia in the retina of a Slc7a7-deficient zebrafish larva from 2.5 dpf. Time-lapse confocal imaging starting by 54 hpf of a *Tg(mpeg1:gal4; uas:Nfsb-mCherry)* larva injected with the slc7a7-sp22 morpholino at the 1-2 cell stage, and imaged in parallel with the control Mo-injected larva shown in Movie 3, in the same glass-bottomed dish. Lateral view (maximum projection from a z-stack); time step = 3 min.

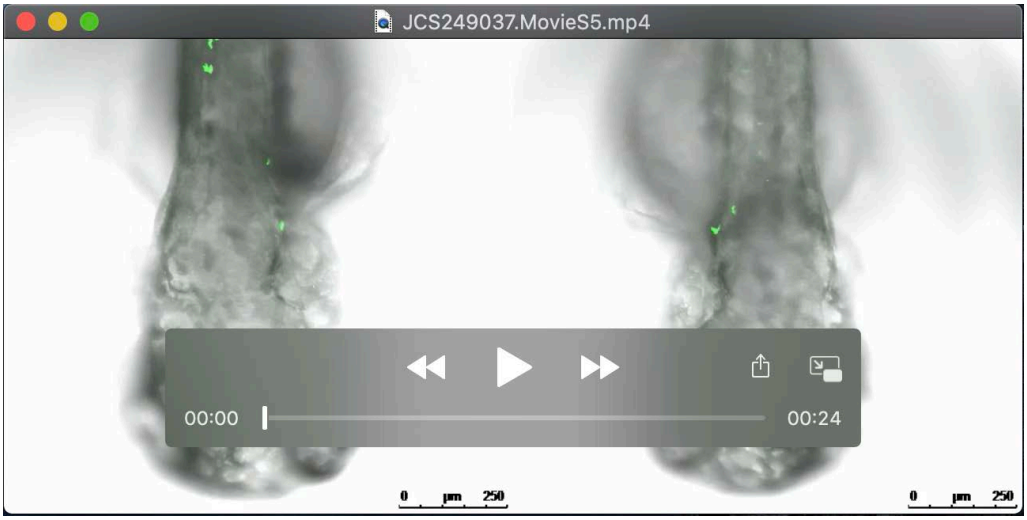

Movie 5 (related to Fig. 3D,E). Neutrophils infiltrate the midbrain optic tectum in Slc7a7-deficient larvae by 3 dpf. Parallel time-lapse confocal imaging of *Tg(mpx:GFP)* 3 dpf larvae injected with slc7a7-sp22 Mo (left) or control Mo (right) at the 1-2 cell stage. Time is indicated in the upper right corner; time step = 5 min.

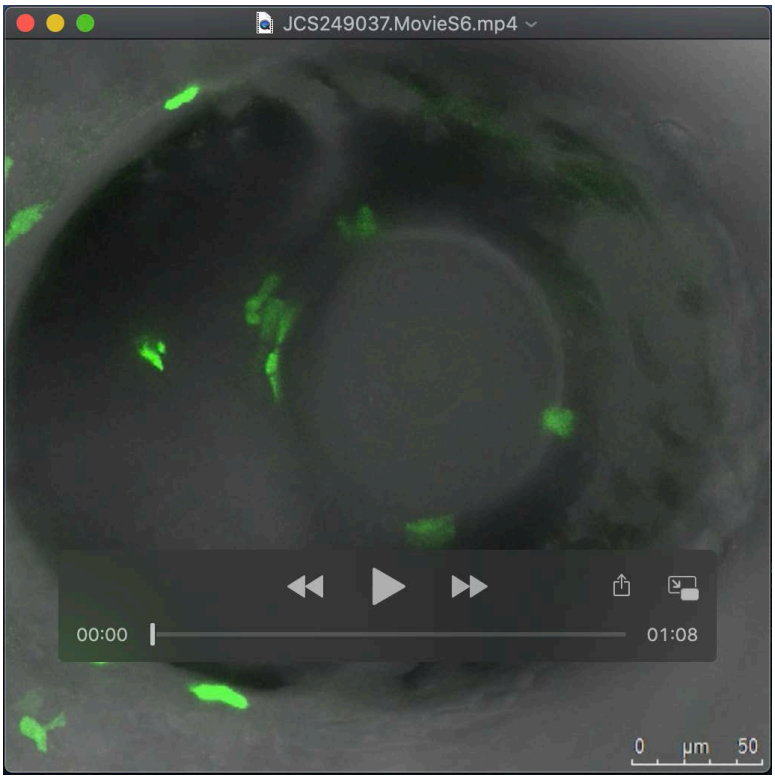

Movie 6 (related to Fig. 3F). Neutrophils infiltrate the retina in Slc7a7-deficient larvae by 3 dpf. Time-lapse confocal imaging of a *Tg(mpx:GFP)* 3 dpf larva injected with the slc7a7-sp22 Mo at the 1-2 cell stage. Lateral view of the eye (maximum projection from a z-stack); time step = 1 min.

Movie 7 (related to Fig. 3G). The optic tectum of WT larvae contains no neutrophils. Z-scroll in dorsal view, rostral to the left, through a confocal z-stack spanning the entire OT of a WT *Tg(mpeg1mCherry; mpx:GFP)* sibling of the mutant larva shown in Movie 8. Neutrophils appear only towards the end of the z-scroll, in intersititial tissue outsied the brain. In the left panel, the bright-field channel is superimposed on the red and green fluorescence channels so as to show anatomical contours; the right panel shows only the overlay of red and green fuorescence channels so as to see these signals better.

Movie 8 (related to Fig. 3H). Neutrophils in the optic tectum of Slc7a7-deficient larvae interact with the dying microglia. Z-scroll in dorsal view, rostral to the left, through a confocal z-stack spanning the entire OT of a *cerise* mutant *Tg(mpeg1:mCherry; mpx:GFP)* larva at 4 dpf. Neutrophils (green) appear throughout the OT, in close correlation with dying microglia (red). In the left panel, the bright-field channel is superimposed on the red and green fluorescence channels so as to show anatomical contours; the right panel shows only the overlay of red and green fuorescence channels so as to see these signals better.